Quantum theory of a bandpass Purcell filter for qubit readout

Eyob A. Sete,[1,*] John M. Martinis,[2,3] and Alexander N. Korotkov[1]
[1]*Department of Electrical and Computer Engineering, University of California, Riverside, California 92521, USA*
[2]*Department of Physics, University of California, Santa Barbara, California 93106, USA*
[3]*Google Inc., Santa Barbara, California, USA*
(Received 22 April 2015; published 21 July 2015)

The measurement fidelity of superconducting transmon and Xmon qubits is partially limited by the qubit energy relaxation through the resonator into the transmission line, which is also known as the Purcell effect. One way to suppress this energy relaxation is to employ a filter which impedes microwave propagation at the qubit frequency. We present semiclassical and quantum analyses for the bandpass Purcell filter realized by E. Jeffrey *et al.* [Phys. Rev. Lett. **112**, 190504 (2014)]. For typical experimental parameters, the bandpass filter suppresses the qubit relaxation rate by up to two orders of magnitude while maintaining the same measurement rate. We also show that in the presence of a microwave drive the qubit relaxation rate further decreases with increasing drive strength.

DOI: 10.1103/PhysRevA.92.012325 PACS number(s): 03.67.Lx, 85.25.−j, 03.65.Yz

I. INTRODUCTION

The implementation of fault-tolerant quantum information processing [1] requires high-fidelity quantum gates and also needs sufficiently fast and accurate qubit measurement. Superconducting quantum computing technology [2–10] is currently approaching the threshold for quantum error correction. Compared with the recent rapid progress in the increase of single-qubit and two-qubit gate fidelities, qubit measurement shows somewhat slower progress. The development of faster and higher-fidelity qubit readout remains an important task.

In circuit QED (cQED) [11,12] the qubit state is inferred by measuring the state-dependent frequency shift of the resonator via homodyne detection. This method introduces an unwanted decay channel [13] for the qubit due to the energy leakage through the resonator into the transmission line, the process known as the Purcell effect [14,15]. The Purcell effect is one of the limiting factors for high fidelity qubit readout.

In principle, the Purcell rate can be suppressed by increasing the qubit-resonator detuning, decreasing the qubit-resonator coupling, or decreasing the resonator bandwidth due to damping. However, these simple methods increase the time needed to measure the qubit. This leads to a trade-off between the qubit relaxation and measurement time, whereas it is desirable to suppress the Purcell rate without compromising qubit measurement. Several proposals have been put forward for this purpose, which include employing a Purcell filter [16–19], engineering a Purcell-protected qubit [20,21], or using a tunable coupler that decouples the transmission line from the resonator during the qubit-resonator interaction, thereby avoiding the Purcell effect altogether [22].

The general idea of the Purcell filter is to impede the propagation of the photon emitted at the qubit frequency, compared with propagation of the microwave field at the resonator frequency, used for the qubit measurement. A notch (band-rejection) filter detuned by 1.7 GHz from the resonator frequency was realized in Ref. [16]. A factor of 50 reduction in the Purcell rate was demonstrated when the qubit frequency was placed in the rejection band of the filter. A bandpass filter with the quality factor $Q_f \simeq 30$ (and corresponding bandwidth of 0.22 GHz) centered near the resonator frequency was used in Ref. [17]. This allowed the qubit measurement within 140 ns with fidelities $F_{|1\rangle} = 98.7$ and $F_{|0\rangle} = 99.3$ for the two qubit states. (The bandpass Purcell filter was also used in Ref. [10]; it had a similar design with a few minor changes.) A major advantage of the bandpass Purcell filter in comparison with the notch filter is the possibility to keep strongly reduced Purcell rate for qubits with practically any frequency (except near the filter frequency), thus allowing quantum gates based on tuning the qubit frequency, and also allowing multiplexed readout of several qubits by placing readout resonators with different frequencies within the filter bandwidth.

In this work we analyze the Purcell filter of Ref. [17] using both semiclassical and quantum approaches and considering both the weak and the strong drive regimes. Our semiclassical analysis uses somewhat different language compared to the analysis in Ref. [17]; however, the results are very similar (they show that with the filter the Purcell rate can be suppressed by two orders of magnitude, while maintaining the same measurement time). The results of the quantum analysis in the regime of a weak measurement drive or no drive (considering the single-photon subspace) practically coincide with the semiclassical results. In the presence of strong microwave drive, the Purcell rate is further suppressed with increasing drive strength. We have found that this suppression is stronger than that obtained without a filter [23].

In Sec. II we discuss the general idea of the bandpass Purcell filter and analyze its operation semiclassically. Section III is devoted to the quantum calculation of the Purcell rate in the presence of the bandpass Purcell filter. In Sec. IV we discuss further suppression of the Purcell rate due to an applied microwave drive. Section V is the conclusion. In the Appendix we review the basic theory of a transmon/Xmon qubit measurement, the Purcell decay, and the corresponding measurement error without the Purcell filter.

*Present address: Rigetti Quantum Computing, 2855 Telegraph Ave, Berkeley, CA 94705, USA.

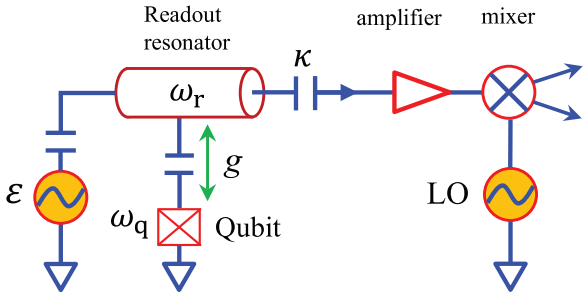

FIG. 1. (Color online) Schematic of a standard circuit QED qubit readout setup. The qubit state slightly changes the resonator frequency ω_r (due to qubit-resonator interaction with strength g), and this is sensed by passing the microwave through (or reflecting from) the resonator. The amplified outgoing microwave is combined with the local oscillator at the mixer, whose output is measured to discriminate the qubit states. The energy decay κ of the resonator is mainly due to its coupling with the transmission line.

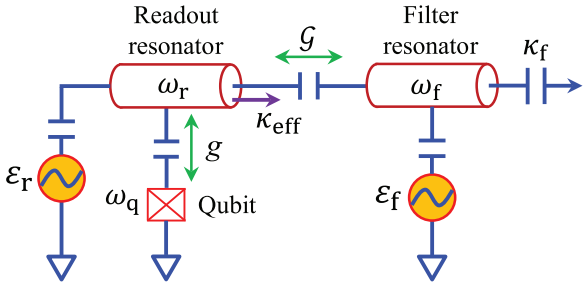

FIG. 2. (Color online) Qubit measurement schematic with the bandpass Purcell filter of Ref. [17]. The readout resonator with frequency ω_r (which depends on the qubit state) is coupled (coupling $\mathcal{G}$) with a filter resonator of frequency ω_f, which decays into the transmission line with the rate κ_f. The further processing of the outgoing microwave (not shown) is the same as in Fig. 1. The microwave drive can be applied either to the readout (ε_r) or to the filter (ε_f) resonators. Coupling with the decaying filter resonator produces an effective decay rate κ_{eff} of the readout resonator, which depends on the drive frequency. As a result, for the measurement microwave $\kappa_{eff} = \kappa_r$, while the qubit sees a much smaller value $\kappa_{eff} = \kappa_q$, thus leading to a suppression of the qubit Purcell decay by a factor κ_q/κ_r.

II. IDEA OF A BANDPASS PURCELL FILTER AND SEMICLASSICAL ANALYSIS

In the standard cQED setup of dispersive measurement (Fig. 1) the qubit interaction with the resonator slightly changes the effective resonator frequency depending on the qubit state, so that it is $\omega_r^{|e\rangle}$ when the qubit is in the excited state and $\omega_r^{|g\rangle}$ when the qubit is in the ground state. The dispersive coupling χ is defined as

$$\chi \equiv \left(\omega_r^{|e\rangle} - \omega_r^{|g\rangle}\right)/2. \tag{1}$$

In the two-level approximation for the qubit, $\chi = g^2/(\omega_q^b - \omega_r^b)$, where g is the qubit-resonator coupling and ω_q^b and ω_r^b are the bare frequencies of the qubit and the resonator, respectively [11]. For a transmon or an Xmon qubit, χ is usually significantly smaller, $\chi \approx -g^2\delta_q/[(\omega_q^b - \omega_r^b)(\omega_q^b - \delta_q - \omega_r^b)]$, where δ_q is the qubit anharmonicity ($\delta_q > 0$); moreover, χ as well as the central frequency $(\omega_r^{|e\rangle} + \omega_r^{|g\rangle})/2$ depend on the number of photons n in the resonator (see [24,25] and the Appendix for a more detailed discussion). The resonator frequency change (and thus the qubit state) is sensed by applying the microwave field with amplitude ε, then amplifying the transmitted or reflected signal, and then mixing it with the applied microwave field to measure its phase and amplitude (Fig. 1).

In the process of measurement, the qubit decays with the Purcell rate [11]

$$\Gamma \approx \kappa \frac{g^2}{(\omega_q - \omega_r)^2}, \tag{2}$$

where κ is the resonator energy damping rate (mostly due to leakage into the transmission line, see Fig. 1). Note that in this formula we do not distinguish the bare and effective frequencies. In the quantum language this can be interpreted as the leakage with the rate κ of the qubit "tail" $g^2/(\omega_q - \omega_r)^2$, existing in the form of the resonator photon. However, the Purcell decay also has a simple classical interpretation via the resistive damping [13], essentially being a linear effect, in contrast to the dispersion (1)—see the Appendix for more details, including dependence of Γ on n [23].

The Purcell decay leads to measurement error; therefore, it is important to reduce the rate Γ. This can be done by decreasing the ratio $g/|\omega_q - \omega_r|$; however, this decreases χ and thus increases the necessary measurement time t_m (see Appendix for more details). Another way to decrease Γ is to use a very small leakage rate κ; however, this also increases the measurement time t_m because the ring-up and ring-down processes give a natural limitation $t_m \gtrsim 4\kappa^{-1}$, and in many practical cases it is even $t_m \gg 10\kappa^{-1}$.

It would be good if the rate κ which governs the measurement time were different from κ in Eq. (2): specifically if κ for the Purcell decay were much smaller than κ for the measurement. This is exactly what is achieved by using the bandpass filter of Ref. [17]. There are other ways to explain how this Purcell filter works [17], but here we interpret the main idea of the bandpass Purcell filter as producing different effective rates κ_{eff} for the measurement and for the Purcell decay (so that the measurement microwave easily passes through the filter, while the propagation of the photon emitted by the qubit is strongly impeded by the filter).

The schematic of the qubit measurement with the bandpass Purcell filter of Ref. [17] is shown in Fig. 2. Besides the readout resonator with qubit-state-dependent frequency $\omega_r = \omega_r^{|e\rangle}$ or $\omega_r = \omega_r^{|g\rangle}$, there is a second (filter) resonator with frequency ω_f, coupled with the readout resonator with the coupling $\mathcal{G}$. (The coupling $\mathcal{G}$ is inductive, but we draw it as capacitive to keep the figure simple.) The filter resonator leaks the microwave into the transmission line with a relatively large damping rate κ_f, so that its Q factor is $Q_f = \omega_f/\kappa_f \simeq 30$, while $|\mathcal{G}| \ll \kappa_f$. The leaked field is then amplified and sent to the mixer (not shown) in the same way as in the standard cQED setup. The readout and filter resonators are in general detuned from each other, but not much, $|\omega_r - \omega_f| \lesssim \kappa_f$ (detuning is needed to multiplex readout of several qubits using the same filter resonator [10,17]; for simplicity we consider the measurement of only one qubit). The filter resonator is pumped with the drive frequency ω_d

(close to ω_r) and amplitude ε_f. However, for us it will be easier to first assume instead that the readout resonator is pumped with amplitude ε_r (Fig. 2), and then show the correspondence between the drives ε_r and ε_f.

Let us use the rotating wave approximation [26,27] with the rotating frame $e^{-i\omega_d t}$ based on the drive frequency ω_d. Then the evolution of the *classical* field amplitudes $\alpha(t)$ and $\beta(t)$ in the readout and filter resonators, respectively, is given by the equations

$$\dot{\alpha} = -i\Delta_{rd}\alpha - i\mathcal{G}\beta - i\varepsilon_r, \tag{3}$$

$$\dot{\beta} = -i\Delta_{fd}\beta - i\mathcal{G}^*\alpha - \frac{\kappa_f}{2}\beta, \tag{4}$$

where α and β are normalized so that $|\alpha|^2$ and $|\beta|^2$ are the average number of photons in the resonators, ε_r is normalized correspondingly, and

$$\Delta_{rd} = \omega_r - \omega_d, \quad \Delta_{fd} = \omega_f - \omega_d \tag{5}$$

(recall that ω_r depends on the qubit state). If we are not interested in the details of evolution on the fast time scale κ_f^{-1}, then we can use the quasisteady state for β [obtained from Eq. (4) using $\dot{\beta} = 0$],

$$\beta = \frac{-i\mathcal{G}^*}{\kappa_f/2 + i\Delta_{fd}}\alpha, \tag{6}$$

which can then be inserted into Eq. (3), giving

$$\dot{\alpha} = -i(\Delta_{rd} + \delta\omega_r)\alpha - \frac{\kappa_{eff}}{2}\alpha - i\varepsilon_r, \tag{7}$$

$$\kappa_{eff} = \frac{4|\mathcal{G}|^2}{\kappa_f}\frac{1}{1 + (2\Delta_{fd}/\kappa_f)^2}, \tag{8}$$

$$\delta\omega_r = -\frac{|\mathcal{G}|^2\Delta_{fd}}{(\kappa_f/2)^2 + \Delta_{fd}^2} = -\frac{\Delta_{fd}}{\kappa_f}\kappa_{eff}. \tag{9}$$

Thus we see that the field α evolves in practically the same way as in the standard setup of Fig. 1; however, interaction with the filter resonator shifts the readout resonator frequency by $\delta\omega_r$ and introduces the effective leakage rate κ_{eff} of the readout resonator.

Most importantly, κ_{eff} depends on the drive frequency. For measurement we use $\omega_d \approx \omega_r$, so κ_{eff} is approximately

$$\kappa_r \equiv \frac{4|\mathcal{G}|^2}{\kappa_f}\frac{1}{1 + [2(\omega_r - \omega_f)/\kappa_f]^2}. \tag{10}$$

However, when the qubit tries to leak its excitation through the readout resonator, this can be considered as a drive at the qubit frequency, $\omega_d = \omega_q$, and the corresponding κ_{eff} is then

$$\kappa_q \equiv \frac{4|\mathcal{G}|^2}{\kappa_f}\frac{1}{1 + [2(\omega_q - \omega_f)/\kappa_f]^2}, \tag{11}$$

which is much smaller than κ_r if the qubit is detuned away from the filter linewidth, $|\omega_q - \omega_f| \gg \kappa_f$. This difference is exactly what we wished for suppressing the Purcell rate Γ: the measurement is governed by κ_r, while the qubit sees a much smaller value κ_q. Therefore, we would expect that the Purcell rate is given by Eq. (2) with $\kappa = \kappa_q$ [see Eq. (32) later], while the "separation" measurement error is given by Eqs. (A36)–(A38) with $\kappa = \kappa_r$ (see Appendix). As a result, compared with the standard setup (Fig. 1) with the same physical parameters for measurement, the Purcell rate is suppressed by the factor

$$F = \frac{\kappa_q}{\kappa_r} = \frac{1 + [2(\omega_r - \omega_f)/\kappa_f]^2}{1 + [2(\omega_q - \omega_f)/\kappa_f]^2} \ll 1. \tag{12}$$

This is essentially the *main result* of this paper, which will be confirmed by the quantum analysis in the next section. (To avoid a possible confusion, we note that κ_q is not the qubit decay rate; it is the resonator decay, as seen by the qubit.)

Our result for the Purcell suppression factor was based on the behavior of the field amplitude in the readout resonator. Let us also check that the field γ_{tl} propagating in the outgoing transmission line behaves according to the effective model as well. The outgoing field amplitude is $\gamma_{tl} = \sqrt{\kappa_f}\,\beta$ (in the normalization for which $|\gamma_{tl}|^2$ is the average number of propagating photons per second). Using Eq. (6) we find

$$\gamma_{tl} = \frac{-i\mathcal{G}^*\sqrt{\kappa_f}}{\kappa_f/2 + i\Delta_{fd}}\alpha = e^{i\varphi}\sqrt{\kappa_{eff}}\,\alpha, \tag{13}$$

so, as expected, the outgoing amplitude behaves as in the standard setup of Fig. 1 with $\kappa = \kappa_{eff}$, up to an unimportant phase shift $\varphi = \arg[-i\mathcal{G}^*/(\kappa_f/2 + i\Delta_{fd})]$. Note that to show the equivalence between the dynamics (including transients) of the systems in Figs. 1 and 2 we needed the assumption of a sufficiently large κ_f in order to use the quasisteady state (6). However, this assumption is not needed if we consider only the steady state (without transients).

So far we assumed that the measurement is performed by driving the readout resonator with the amplitude ε_r. Now let us consider the realistic case [10,17] when the drive ε_f is applied to the filter resonator. The evolution equations (3) and (4) for the classical field amplitudes are then replaced by

$$\dot{\alpha} = -i\Delta_{rd}\alpha - i\mathcal{G}\beta, \tag{14}$$

$$\dot{\beta} = -i\Delta_{fd}\beta - i\mathcal{G}^*\alpha - \frac{\kappa_f}{2}\beta - i\varepsilon_f, \tag{15}$$

so that the quasisteady state for the filter resonator is

$$\beta = \frac{-i\mathcal{G}^*}{\kappa_f/2 + i\Delta_{fd}}\alpha + \frac{-i\varepsilon_f}{\kappa_f/2 + i\Delta_{fd}}, \tag{16}$$

and the field evolution in the readout resonator is

$$\dot{\alpha} = -i(\Delta_{rd} + \delta\omega_r)\alpha - \frac{\kappa_{eff}}{2}\alpha - \frac{\mathcal{G}}{\kappa_f/2 + i\Delta_{fd}}\varepsilon_f, \tag{17}$$

with the same κ_{eff} and $\delta\omega_r$ given by Eqs. (8) and (9). The only difference between the effective evolution equations (7) and (17) is a linear relation,

$$\varepsilon_r \leftrightarrow -i\varepsilon_f\mathcal{G}/(\kappa_f/2 + i\Delta_{fd}), \tag{18}$$

between the drive amplitudes ε_r and ε_f producing the same effect. Therefore, our results obtained above remain unchanged for driving the filter resonator, and the Purcell rate suppression factor is still given by Eq. (12).

Note that in the quasisteady state the separation between the filter amplitudes β for the two qubit states does not depend on whether the drive is applied to the filter or readout resonator, as long as we use the correspondence (18) between the drive amplitudes. The same is true for the separation between the outgoing fields γ_{tl}. Similarly, the separation between the

outgoing fields for the two qubit states is the same (up to the phase φ) as in the standard setup of Fig. 1 with $\varepsilon = \varepsilon_r$, $\kappa = \kappa_r$, and the resonator frequency adjusted by $\delta\omega_r$ given by Eq. (9). Therefore, these configurations are equivalent to each other from the point of view of quantum measurement, including interaction between the qubit and readout resonator, extraction of quantum information, back-action, etc.

Nevertheless, driving the filter resonator produces a different outgoing field $\gamma_{tl} = \sqrt{\kappa_f}\,\beta$, which now contains an additional term $-i\varepsilon_f\sqrt{\kappa_f}/(\kappa_f/2 + i\Delta_{fd})$ in comparison with Eq. (13), which comes from the second term in Eq. (16). In particular, instead of the Lorentzian line shape of the transfer function when driving the readout resonator, the transfer function for driving the filter is (in the steady state)

$$\frac{\gamma_{tl}^{(f)}}{\varepsilon_f} = \frac{\sqrt{\kappa_f}}{\kappa_f/2 + i\Delta_{fd}} \frac{2\Delta_{rd}/\kappa_{eff}}{1 + \dfrac{2i(\Delta_{rd} + \delta\omega_r)}{\kappa_{eff}}}, \tag{19}$$

where κ_{eff} can be replaced with κ_r. (Note a nonstandard normalization of the transfer function because of different normalizations of $\gamma_{tl}^{(f)}$ and ε_f.) This line shape for the amplitude $|\gamma_{tl}^{(f)}/\varepsilon_f|$ shows a dip near ω_r (note that $\gamma_{tl}^{(f)}/\varepsilon_f = 0$ at $\omega_d = \omega_r$) and is significantly asymmetric when $\delta\omega_r$ is comparable to κ_r; this occurs when the detuning between the readout and filter resonators is comparable to κ_f—see Eq. (9). In terms of the field α in the readout resonator, the outgoing field at steady state is

$$\gamma_{tl}^{(f)} = -\frac{\sqrt{\kappa_f}\,\Delta_{rd}}{\mathcal{G}}\,\alpha \tag{20}$$

instead of Eq. (13) for driving the readout resonator.

The difference between the outgoing fields $\gamma_{tl}^{(f)}$ and $\gamma_{tl}^{(r)}$ when driving the filter or readout resonator (for the same α, i.e., the same measurement conditions) may be important for saturation of the microwave amplifier. The ratio of the corresponding outgoing powers is

$$\frac{\left|\gamma_{tl}^{(f)}\right|^2}{\left|\gamma_{tl}^{(r)}\right|^2} = \left(\frac{\Delta_{rd}}{\kappa_r}\right)^2 \frac{4}{1 + (2\Delta_{fd}/\kappa_f)^2}, \tag{21}$$

where we assumed $|\Delta_{rd}| \ll \kappa_f$ (so that $\kappa_{eff} \approx \kappa_r$). For example, if the drive frequency is chosen as $\omega_d = (\omega_r^{|g\rangle} + \omega_r^{|e\rangle})/2$, then $\Delta_{rd} = \pm\chi$; if in this case $|\chi| \ll \kappa_r$, then driving the filter resonator is advantageous because it produces less power to be amplified, while driving the readout resonator is advantageous if $|\chi| \gg \kappa_r$. However, when $\omega_d \neq (\omega_r^{|g\rangle} + \omega_r^{|e\rangle})/2$, the situation is more complicated.

Figure 3 shows the transient phase-space evolution $\beta(t)$ of the field (coherent state) in the filter resonator when a step-function drive is applied to the readout resonator (red curves) or to the filter resonator (blue curves), with the drive amplitudes related via Eq. (18), and for real ε_r. The solid curves show the evolution when the qubit is in the excited state, while the dashed curves are for the qubit in the ground state. We have used parameters similar to the experimental parameters of Ref. [17]: $\omega_r^{|e\rangle}/2\pi = 6.8$ GHz, $\omega_r^{|g\rangle}/2\pi = 6.803$ GHz (so that $2\chi/2\pi = -3$ MHz), $\omega_f/2\pi = 6.75$ GHz, $Q_f = 30$ (so that $\kappa_f^{-1} = 0.71$ ns), and $\kappa_r^{-1} = 30$ ns (so that $\mathcal{G}/2\pi = 18.9$ MHz). The field evolution is calculated using either Eqs. (3) and (4) or Eqs. (14) and (15); in simulations we have neglected the dependence of χ and $(\omega_r^{|e\rangle} + \omega_r^{|g\rangle})/2$ on the average number of photons $\bar{n}_r = |\alpha|^2$ in the readout resonator (see Appendix). The black dots indicate the time moments every 10 ns between 0 and 100 ns, and then every 50 ns. The circles illustrate the coherent state error circles [28] in the steady state. We see that when the drive is applied to the filter resonator (blue curves), the evolution $\beta(t)$ is initially very fast (governed by κ_f), while after the quasisteady state is reached, the evolution is governed by a much slower κ_r, eventually approaching the steady state. When the drive is applied to the readout resonator (red curves), the transient evolution is always governed by the slower decay κ_r.

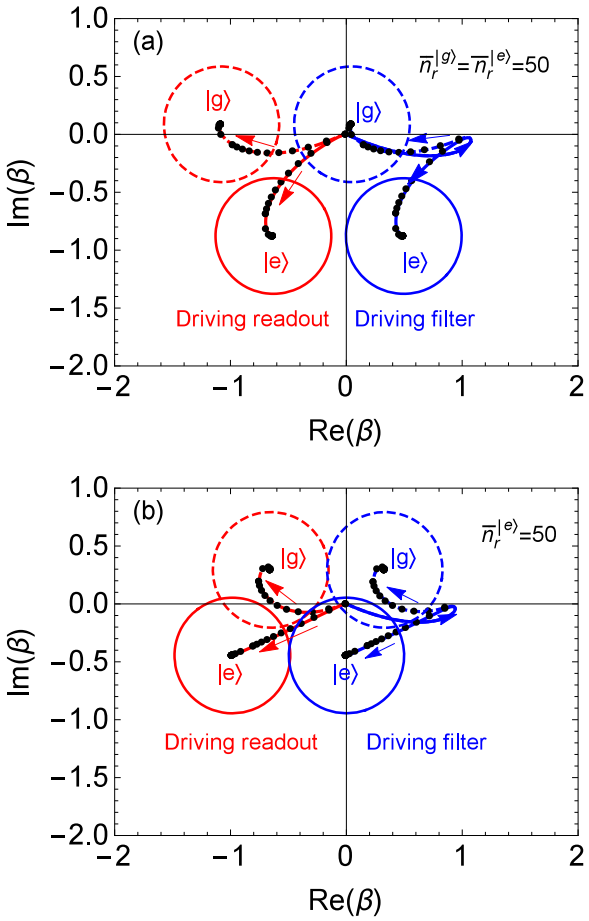

FIG. 3. (Color online) Phase-space transient evolution of qubit-state-dependent coherent states in the filter resonator for driving either the readout resonator (red curves, left) or the filter (blue curves, right), with the drive amplitudes related via Eq. (18). Solid curves are for the qubit state $|e\rangle$, dashed curves are for the state $|g\rangle$. See text for the assumed parameters. For (a) we choose the drive frequency ω_d symmetrically for the readout resonator, so that $\bar{n}_r^{|g\rangle} = \bar{n}_r^{|e\rangle} = 50$. For (b) we choose ω_d symmetrically for the filter resonator, so that $\bar{n}_f^{|g\rangle} = \bar{n}_f^{|e\rangle}$ when driving the filter; we choose $\bar{n}_r^{|e\rangle} = 50$. The black dots indicate time moments in the evolution every 10 ns until 100 ns, then every 50 ns. Circles illustrate the coherent state error circles in the steady state.

In Fig. 3(a) we choose the drive frequency ω_d symmetrically from the point of view of the readout resonator field, so that

in the steady state $\bar{n}_r^{|g\rangle} = \bar{n}_r^{|e\rangle} = 50$, where $\bar{n}_r^{|g\rangle}$ and $\bar{n}_r^{|e\rangle}$ are the average photon numbers for the two qubit states. For that we need $\omega_d = (\omega_r^{|g\rangle} + \omega_r^{|e\rangle})/2 + \delta\omega_r$ with $\delta\omega_r$ given by Eq. (9); for our parameters $\delta\omega_r/2\pi = 1.23$ MHz, so $\omega_d/2\pi = 6.80273$ GHz. Such symmetric choice of the drive frequency provides the largest separation between the two coherent states for a fixed drive amplitude if $2|\chi| < \kappa_r$. While the field in the readout resonator is always symmetric in this case, Fig. 3(a) shows that the field in the filter resonator is symmetric only when driving the readout resonator (red curves, $\bar{n}_f^{|g\rangle} = \bar{n}_f^{|e\rangle} = 1.2$), while it is strongly asymmetric when the filter resonator is driven (blue curves, $\bar{n}_f^{|g\rangle} = 0.01$, $\bar{n}_f^{|e\rangle} = 1.0$; $\bar{n}_f^{|g\rangle}$ is very small because for our parameters $\delta\omega_r \approx |\chi|$ and therefore $\omega_d \approx \omega_r^{|g\rangle}$). The number of photons in the filter is much less than in the readout resonator because $\kappa_f \gg \kappa_r$.

In Fig. 3(b) we choose ω_d so that in the steady state $\bar{n}_f^{|g\rangle} = \bar{n}_f^{|e\rangle}$ for driving the filter; this is the natural choice for decreasing the microwave power to be amplified. This occurs at $\omega_d/2\pi = 6.80120$, which is close to the expected value $(\omega_r^{|g\rangle} + \omega_r^{|e\rangle})/2$, but not equal because of the asymmetry of the line shape (19). We choose the amplitudes to produce $\bar{n}_r^{|e\rangle} = 50$ (then $\bar{n}_r^{|g\rangle} = 22$). The difference between $\bar{n}_r^{|e\rangle}$ and $\bar{n}_r^{|g\rangle}$ leads to different values $\bar{n}_f^{|e\rangle} = 1.2$ and $\bar{n}_f^{|g\rangle} = 0.5$ when driving the readout resonator, while for driving the filter the field in the filter is symmetric, $\bar{n}_f^{|e\rangle} = \bar{n}_f^{|g\rangle} = 0.2$. Compared to the case of Fig. 3(a), there is 5 times less power to be amplified for the $|e\rangle$ state (when driving the filter); however, the state separation is 1.3 times smaller (in amplitude) for the same $\bar{n}_r^{|e\rangle}$. Thus, there is a trade-off between the state separation and amplified power in choosing the drive frequency. Comparing the red and blue curves in Fig. 3(b), we see that in the steady state $\bar{n}_f^{|g\rangle}$ and $\bar{n}_f^{|e\rangle}$ are smaller for driving the filter rather than the readout resonator. This is beneficial because there is less power to be amplified; however, the ratio is not very big (as expected for a moderate value $|\chi|/\kappa_r = 0.28$).

Note that our definition of κ_r in Eq. (10) is not strictly well defined because the resonator frequency ω_r depends on the qubit state, and the drive frequency can be in between $\omega_r^{|e\rangle}$ and $\omega_r^{|g\rangle}$. However, this frequency difference is much smaller than κ_f, and therefore not important for practical purposes in the definition of κ_r. In an experiment κ_r can be measured either via the field decay [17] or via the linewidth of the steady-state transfer function showing the dip of $|\gamma_{tl}^{(f)}/\varepsilon_f|$ near the resonance $\omega_d = \omega_r$ [Eq. (19)], since near the dip $\kappa_{eff} \approx \kappa_r$.

Thus far we assumed that all decay κ_f in the filter resonator is due to the leakage κ_f^{out} into the outgoing transmission line. If $\kappa_f^{out} < \kappa_f$ and the decay $\kappa_f - \kappa_f^{out}$ is due to leakage into the line delivering the drive ε_f or due to another dissipation channel, then the only difference compared to the previous discussion is the extra factor $\sqrt{\kappa_f^{out}/\kappa_f}$ for the outgoing field γ_{tl}. This will lead to multiplication of the overall quantum efficiency of the measurement by κ_f^{out}/κ_f and will only slightly affect the measurement fidelity. Adding dissipation in the readout resonator with rate $\kappa_{r,d}$ increases the effective linewidth to $\kappa_{eff} + \kappa_{r,d}$ and multiplies the quantum efficiency by $\kappa_r/(\kappa_r + \kappa_{r,d})$. Most importantly, since $\kappa_{r,d}$ does not change with frequency, the Purcell suppression factor (12) becomes $(\kappa_q + \kappa_{r,d})/(\kappa_r + \kappa_{r,d})$, so that the Purcell filter performance deteriorates; we will discuss this in a little more detail in Sec. III C.

Note that our main result (12) for the Purcell suppression factor is slightly different from the result $F = [\kappa_f/2(\omega_q - \omega_r)]^2(\omega_q/\omega_r)^2$, which was derived in Ref. [17] using the circuit theory. The reasons are the following. First, in the derivation of [17] it was assumed that the two resonators have the same frequency, which makes the numerator in Eq. (12) equal to 1. Second, the term 1 in the denominator in Eq. (12) was essentially neglected in comparison with the larger second term. Finally, the role of the factor $(\omega_q/\omega_r)^2$ is not quite clear. In the derivation of Ref. [17] keeping this factor was exceeding the accuracy of the derivation, while in our derivation we essentially use the rotating wave approximation, which assumes $\omega_q/\omega_r \approx 1$. Aside from these small differences, our result coincides with the result of Ref. [17].

III. QUANTUM ANALYSIS IN SINGLE-EXCITATION SUBSPACE

In this section we discuss the quantum derivation of the Purcell rate in the presence of the bandpass filter in the regime when the resonators are not driven or driven sufficiently weakly to neglect dependence of the Purcell rate on the number of photons in the resonator [23]. More precisely, we consider the quantum evolution in the single-excitation (and zero-excitation) subspace. We apply two methods: the wave function approach, in which we use a non-Hermitian Hamiltonian with a decaying wave function, and the more traditional density matrix analysis.

In the absence of the drive and in the rotating wave approximation, the relevant Hamiltonian of the system shown in Fig. 2 (without considering decay κ_f) is ($\hbar = 1$)

$$H = \omega_q^b \sigma_+\sigma_- + \omega_r^b a^\dagger a + \omega_f b^\dagger b + g(a^\dagger\sigma_- + a\sigma_+) + \mathcal{G}a^\dagger b + \mathcal{G}^* a b^\dagger, \tag{22}$$

where ω_q^b is the bare qubit frequency, ω_r^b is the bare frequency of the readout resonator, ω_f is the filter resonator frequency, raising/lowering operators σ_+ and σ_- act on the qubit state, $a^\dagger$ and a are the creation and annihilation operators for the readout resonator, $b^\dagger$ and b are for the filter resonator, g is the qubit-readout resonator coupling, and $\mathcal{G}$ is the resonator-resonator coupling. For simplicity we assume a real positive g, but $\mathcal{G}$ can be complex for generality (for the capacitive or inductive coupling between the resonators, $\mathcal{G}$ is real if the same generalized coordinates are used for both resonators).

Note that in the case without drive it is sufficient to consider only two levels for the qubit because only the single-excitation (and zero-excitation) subspace is involved in the evolution, and therefore the amount of qubit nonlinearity due to the Josephson junction is irrelevant. However, in the presence of a drive (considered in the next section) it is formally necessary to take into account several levels in the qubit (as done in the Appendix). Nevertheless, to leading order the Purcell rate is insensitive to this, because the Purcell decay is essentially a classical linear effect (see discussion in the Appendix). Also note that the laboratory-frame Hamiltonian

(22) assumes the rotating wave approximation (as in the standard Jaynes-Cummings Hamiltonian), since it neglects the "counter-rotating" terms of the form $a^\dagger\sigma_+$, $a\sigma_-$, $a^\dagger b^\dagger$, and ab. This requires assumption that $|\omega_q^b - \omega_r^b|$, $|\omega_f - \omega_r^b|$, g, and $|\mathcal{G}|$ are small compared to ω_r^b.

Let us choose the rotating frame with frequency ω_q^b, i.e., $H_0{=}\omega_q^b(\sigma_+\sigma_- + a^\dagger a + b^\dagger b)$; then the interaction Hamiltonian $V = H - H_0$ is

$$V = \Delta_{rq}a^\dagger a + \Delta_{fq}b^\dagger b + g(a^\dagger\sigma_- + a\sigma_+) + \mathcal{G}a^\dagger b + \mathcal{G}^* ab^\dagger, \tag{23}$$

where

$$\Delta_{rq} = \omega_r^b - \omega_q^b, \quad \Delta_{fq} = \omega_f - \omega_q^b, \tag{24}$$

and the interaction picture is equivalent to the Schrödinger picture because $\exp(iH_0t)V\exp(-iH_0t) = V$, which is because the starting Hamiltonian (22) already assumes the rotating-wave approximation. The master equation for the density matrix ρ, which includes the damping κ_f of the filter resonator is

$$\dot\rho = -i[V,\rho] + \kappa_f(b\rho b^\dagger - b^\dagger b\rho/2 - \rho b^\dagger b/2). \tag{25}$$

In general, the bare basis is $|jnm\rangle$, where j represents the qubit states, while n and m represent the readout and filter resonator Fock states, respectively. However, in this section we consider only the single-excitation (and zero-excitation) subspace, so only four bare states are relevant: $|\mathbf{e}\rangle \equiv |e00\rangle$, $|\mathbf{r}\rangle = |g10\rangle$, $|\mathbf{f}\rangle = |g01\rangle$, and $|\mathbf{g}\rangle = |g00\rangle$.

Note that the interaction hybridizes the bare states of the qubit and the resonators. (Hybridization of the readout resonator mode is essentially what makes the qubit measurement possible.) Therefore, when discussing the Purcell rate for the qubit energy relaxation, we actually mean decay of the eigenstate, corresponding to the qubit excited state. This makes perfect sense experimentally, since manipulations of the qubit state usually occur in the eigenbasis (adiabatically, compared with the qubit detuning from the resonator).

A. Method I: Decaying wave function

Instead of using the traditional density matrix language for the description of the Purcell effect [15], it is easier to use the language of wave functions, even in the presence of the decay κ_f [23]. Physically the wave functions can still be used because in the single-excitation subspace unraveling of the Lindblad equation corresponds to only one "no relaxation" scenario (see, e.g., [29]), and therefore the wave function evolution is nonstochastic. Another, more formal way to introduce this language, is to rewrite the master equation (25) as [30,31] $\dot\rho = -i[H_{eff},\rho] + \kappa_f b\rho b^\dagger$, where $H_{eff} = V - i\kappa_f b^\dagger b/2$ is an effective non-Hermitian Hamiltonian. Next, the term $\kappa_f b\rho b^\dagger$ can be neglected because in the single-excitation subspace it produces only an "incoming" contribution from higher-excitation subspaces, which are not populated. Therefore, in the single-excitation subspace we can use $\dot\rho = -i[H_{eff},\rho]$. Equivalently, $|\dot\psi\rangle = -iH_{eff}|\psi\rangle$, which describes the evolution of the *decaying* wave function $|\psi(t)\rangle = c_\mathbf{e}(t)|\mathbf{e}\rangle + c_\mathbf{r}(t)|\mathbf{r}\rangle + c_\mathbf{f}(t)|\mathbf{f}\rangle$. Therefore, the probability amplitudes $c_{\mathbf{e},\mathbf{r},\mathbf{f}}$ satisfy the following equations:

$$\dot c_\mathbf{e} = -igc_\mathbf{r}, \tag{26}$$

$$\dot c_\mathbf{r} = -i\Delta_{rq}c_\mathbf{r} - igc_\mathbf{e} - i\mathcal{G}c_\mathbf{f}, \tag{27}$$

$$\dot c_\mathbf{f} = -i\Delta_{fq}c_\mathbf{f} - i\mathcal{G}^*c_\mathbf{r} - (\kappa_f/2)\,c_\mathbf{f}, \tag{28}$$

while the population $\rho_{\mathbf{gg}}$ of the zero-excitation state $|\mathbf{g}\rangle$ evolves as $\dot\rho_{\mathbf{gg}} = \kappa_f|c_\mathbf{f}|^2$ or can be found as $\rho_{\mathbf{gg}} = 1 - |c_\mathbf{e}|^2 - |c_\mathbf{r}|^2 - |c_\mathbf{f}|^2$. Note that Eqs. (27) and (28) exactly correspond to the classical equations (3) and (4) with Δ_{rd} replaced with Δ_{rq}, also Δ_{fd} replaced with Δ_{fq}, and ε_r replaced with $gc_\mathbf{e}$.

From the eigenvalues $\lambda_{\mathbf{e},\mathbf{r},\mathbf{f}} = -i\omega_{\mathbf{e},\mathbf{r},\mathbf{f}} - \Gamma_{\mathbf{e},\mathbf{r},\mathbf{f}}/2$ of the matrix representing Eqs. (26)–(28), one can obtain the eigenfrequencies $\omega_{\mathbf{e},\mathbf{r},\mathbf{f}}$ and the corresponding decay rates $\Gamma_{\mathbf{e},\mathbf{r},\mathbf{f}}$. These eigenvalues can be found from the qubic equation

$$\lambda^3 + \lambda^2(i\Delta_{rq} + i\Delta_{fq} + \kappa_f/2) + \lambda(-\Delta_{rq}\Delta_{fq} + |\mathcal{G}|^2 + g^2 + i\Delta_{rq}\kappa_f/2) + g^2(i\Delta_{fq} + \kappa_f/2) = 0. \tag{29}$$

We are interested in the Purcell rate $\Gamma = \Gamma_\mathbf{e}$, which corresponds to the decay of the eigenstate close to $|\mathbf{e}\rangle$. Since $\lambda_\mathbf{e}$ is close to zero, in the first approximation we can neglect the term λ^3 in Eq. (29), thus reducing it to the quadratic equation. If more accuracy is needed, the equation can be solved iteratively, replacing λ^3 with the value found in the previous iteration (the second iteration is usually sufficient).

Besides finding the Purcell rate Γ exactly or approximately from Eq. (29), we can find it approximately by using quasisteady solutions of Eqs. (27) and (28), to a large extent following the classical derivation in the previous section. Assuming $\dot c_\mathbf{f} = 0$ in Eq. (28), we find $c_\mathbf{f} = -i\mathcal{G}^*c_\mathbf{r}/(i\Delta_{fq} + \kappa_f/2)$. Inserting this quasisteady value into Eq. (27) and assuming $\dot c_\mathbf{r} = 0$, we find $c_\mathbf{r} = -igc_\mathbf{e}/[i\Delta_{rq} + |\mathcal{G}|^2/(i\Delta_{fq} + \kappa_f/2)]$. Substituting this quasisteady value into Eq. (26), we obtain

$$\dot c_\mathbf{e} = -\frac{g^2}{i\Delta_{rq} + |\mathcal{G}|^2/(i\Delta_{fq} + \kappa_f/2)}\,c_\mathbf{e} = \lambda_\mathbf{e}c_\mathbf{e}. \tag{30}$$

Finally, we obtain the Purcell rate as $\Gamma = -2\mathrm{Re}(\lambda_\mathbf{e})$,

$$\Gamma = \frac{g^2|\mathcal{G}|^2\kappa_f}{\Delta_{rq}^2[(\Delta_{fq} - |\mathcal{G}|^2/\Delta_{rq})^2 + (\kappa_f/2)^2]} \tag{31}$$

$$\approx \frac{g^2|\mathcal{G}|^2\kappa_f}{\Delta_{rq}^2\left[\Delta_{fq}^2 + (\kappa_f/2)^2\right]} = \frac{g^2\kappa_q}{\Delta_{rq}^2}, \tag{32}$$

where κ_q is given by Eq. (11) and we assumed $|\mathcal{G}|^2 \ll \Delta_{fq}\Delta_{rq}$ to transform Eq. (31) into Eq. (32).

The Purcell rate given by Eq. (32) is exactly what we expected from the classical analysis in Sec. II: in the usual formula (2) we simply need to substitute κ with the readout resonator decay rate κ_q seen by the qubit. Since the measurement is governed by a different decay rate κ_r, the effective Purcell rate suppression factor is given by Eq. (12), as was expected. This confirms the results of the classical analysis in Sec. II.

B. Method II: Density matrix analysis

We can also find the Purcell rate in a more traditional way by writing the master equation (25) explicitly in the

single-excitation subspace:

$$\dot{\rho}_{\mathbf{ee}} = ig(\rho_{\mathbf{er}} - \rho_{\mathbf{re}}), \tag{33}$$

$$\dot{\rho}_{\mathbf{er}} = -i\Delta_{\mathrm{qr}}\rho_{\mathbf{er}} - ig(\rho_{\mathbf{rr}} - \rho_{\mathbf{ee}}) + i\mathcal{G}^*\rho_{\mathbf{ef}}, \tag{34}$$

$$\dot{\rho}_{\mathbf{ef}} = -\frac{\kappa_{\mathrm{f}}}{2}\rho_{\mathbf{ef}} - i\Delta_{\mathrm{qf}}\rho_{\mathbf{ef}} + i\mathcal{G}\rho_{\mathbf{er}} - ig\rho_{\mathbf{rf}}, \tag{35}$$

$$\dot{\rho}_{\mathbf{rr}} = -ig(\rho_{\mathbf{er}} - \rho_{\mathbf{re}}) - i\mathcal{G}\rho_{\mathbf{fr}} + i\mathcal{G}^*\rho_{\mathbf{rf}}, \tag{36}$$

$$\dot{\rho}_{\mathbf{rf}} = -\frac{\kappa_{\mathrm{f}}}{2}\rho_{\mathbf{rf}} + i\Delta_{\mathrm{fr}}\rho_{\mathbf{rf}} - i\mathcal{G}\rho_{\mathbf{ff}} + i\mathcal{G}^*\rho_{\mathbf{rr}} - ig\rho_{\mathbf{ef}}, \tag{37}$$

$$\dot{\rho}_{\mathbf{ff}} = -\kappa_{\mathrm{f}}\rho_{\mathbf{ff}} - i\mathcal{G}^*\rho_{\mathbf{rf}} + i\mathcal{G}\rho_{\mathbf{fr}}. \tag{38}$$

Note that $\dot{\rho}_{\mathbf{gg}} = \kappa_{\mathrm{f}}\rho_{\mathbf{ff}}$ and $\rho_{\mathbf{ee}} + \rho_{\mathbf{rr}} + \rho_{\mathbf{ff}} + \rho_{\mathbf{gg}} = 1$ (however, we do not use these two equations for the derivation of the Purcell rate).

Using the quasisteady solutions of Eqs. (34)–(38), i.e., assuming $\dot{\rho}_{\mathbf{er}} = \dot{\rho}_{\mathbf{ef}} = \dot{\rho}_{\mathbf{rr}} = \dot{\rho}_{\mathbf{rf}} = \dot{\rho}_{\mathbf{ff}} = 0$, we can obtain a lengthy equation for $\rho_{\mathbf{er}}$, which is proportional to $\rho_{\mathbf{ee}}$. If we use the first-order expansion of this equation in the coupling g and neglect g^3 terms (there is no g^2 contribution), then

$$\rho_{\mathbf{er}} = \frac{ig}{i\Delta_{\mathrm{rq}} + |\mathcal{G}|^2/(i\Delta_{\mathrm{fq}} + \kappa_{\mathrm{f}}/2)}\,\rho_{\mathbf{ee}}, \tag{39}$$

which has the form similar to Eq. (30). Substituting this $\rho_{\mathbf{er}}$ into Eq. (33), we obtain the evolution equation $\dot{\rho}_{\mathbf{ee}} = -\Gamma\rho_{\mathbf{ee}}$ with Γ given exactly by Eq. (31). If we do not use the above-mentioned approximation for the quasisteady $\rho_{\mathbf{er}}$, then the result for the Purcell rate is slightly different and much lengthier,

$$\Gamma = g^2|\mathcal{G}|^2\kappa_{\mathrm{f}}\big[(\Delta_{\mathrm{rq}}\Delta_{\mathrm{fq}} - |\mathcal{G}|^2)^2 + \big(\Delta_{\mathrm{rq}}^2 + g^2\big)(\kappa_{\mathrm{f}}/2)^2 + g^2\big(\Delta_{\mathrm{fq}}^2 + 2\Delta_{\mathrm{fq}}\Delta_{\mathrm{rq}} - |\mathcal{G}|^2\big) + g^4\big]^{-1}. \tag{40}$$

Thus the derivations based on the wave function and density matrix languages using the quasisteady-state approximation both lead to practically the same result for the Purcell rate Γ. The most physically transparent result is given by Eq. (32), which corresponds to the semiclassical analysis in Sec. II and simply replaces κ in Eq. (2) with κ_{q} seen by the qubit, in contrast to the measurement process, which is governed by κ_{r}.

As an example, let us use the parameters similar to that in Ref. [17]: $\omega_{\mathrm{q}}/2\pi = 5.9$ GHz, $\omega_{\mathrm{r}}/2\pi = 6.8$ GHz, $\omega_{\mathrm{f}}/2\pi = 6.75$ GHz, $Q_{\mathrm{f}} = 30$ (so that $\kappa_{\mathrm{f}}^{-1} = 0.71$ ns), $g/2\pi = 90$ MHz, and $\kappa_{\mathrm{r}}^{-1} = 30$ ns (so that $\mathcal{G}/2\pi = 18.9$ MHz). In this case the resonator decay [Eq. (11)] seen by the qubit is $\kappa_{\mathrm{q}}^{-1} = 1.45\ \mu$s, the Purcell rate [Eq. (32)] is $\Gamma = 1/(145\ \mu\mathrm{s})$, and the Purcell rate suppression factor [Eq. (12)] is $F = 30\ \mathrm{ns}/1.45\ \mu\mathrm{s} = (1 + 0.44^2)/(1 + 7.6^2) = 0.021$.

Thus, for typical parameters the bandpass Purcell filter suppresses the Purcell decay by a factor of ∼50. It is easy to increase this factor to 100 by using $\omega_{\mathrm{q}}/2\pi = 5.5$ GHz in the above example; however, further decrease of the Purcell rate is not needed for practical purposes, while increased resonator-qubit detuning decreases the dispersive shift 2χ (in the above example $2\chi/2\pi \approx -3$ MHz for the qubit anharmonicity of 180 MHz, while for $\omega_{\mathrm{q}}/2\pi = 5.5$ GHz the dispersive shift becomes twice less).

Note that for the parameters in the above example, Eq. (32) overestimates the exact solution for Γ via Eq. (29) by 5%, the same 5% for Eq. (31), and Eq. (40) overestimates the Purcell rate by 2%. The solution of Eq. (29) as a quadratic equation neglecting λ^3 gives Γ, which overestimates the exact solution by 22%, while the second iteration is practically exact (−0.01%). The inaccuracies grow for smaller resonator-qubit detuning (crudely as $\Delta_{\mathrm{rq}}^{-2}$), but remain reasonably small in a sufficiently wide range; for example, Eq. (32) overestimates the Purcell rate by 50% for $\omega_{\mathrm{q}}/2\pi = 6.5$ GHz, i.e. detuning of 0.3 GHz.

C. Nonzero readout resonator damping

In the quantum evolution model (25) we have considered only the damping of the filter resonator with the rate κ_{f}. If there is also an additional energy dissipation in the readout resonator with the rate $\kappa_{\mathrm{r,d}}$ (e.g., due to coupling with the transmission line delivering the drive ε_{r} in Fig. 2), then the master equation (25) should be replaced with

$$\dot{\rho} = -i[V,\rho] + \kappa_{\mathrm{f}}(b\rho b^\dagger - b^\dagger b\rho/2 - \rho b^\dagger b/2) + \kappa_{\mathrm{r,d}}(a\rho a^\dagger - a^\dagger a\rho/2 - \rho a^\dagger a/2). \tag{41}$$

In the wave-function-language derivation this leads to the extra term $-\kappa_{\mathrm{r,d}}c_{\mathbf{r}}/2$ in Eq. (27) for $\dot{c}_{\mathbf{r}}$. This does not change the quasisteady value for $c_{\mathbf{f}}$ but changes the quasisteady value $c_{\mathbf{r}} = -igc_{\mathbf{e}}/[i\Delta_{\mathrm{rq}} + |\mathcal{G}|^2/(i\Delta_{\mathrm{fq}} + \kappa_{\mathrm{f}}/2) + \kappa_{\mathrm{r,d}}/2]$, so that the Purcell rate is

$$\Gamma = 2\,\mathrm{Re}\left[\frac{g^2}{i\Delta_{\mathrm{rq}} + |\mathcal{G}|^2/(i\Delta_{\mathrm{fq}} + \kappa_{\mathrm{f}}/2) + \kappa_{\mathrm{r,d}}/2}\right] \tag{42}$$

$$\approx \frac{g^2(\kappa_{\mathrm{q}} + \kappa_{\mathrm{r,d}})}{\Delta_{\mathrm{rq}}^2} \tag{43}$$

instead of Eq. (32). Practically the same result can be obtained using the derivation via the density matrix evolution (assuming $\kappa_{\mathrm{r,d}} \ll \kappa_{\mathrm{f}}$). As expected, the dissipation $\kappa_{\mathrm{r,d}}$ simply adds to the rate κ_{q} seen by the qubit. Since $\kappa_{\mathrm{r,d}}$ is not affected by the filter, it adds in the same way to the bandwidth κ_{r} governing the qubit measurement process and thus deteriorates the Purcell rate suppression (12), replacing it with $F = (\kappa_{\mathrm{q}} + \kappa_{\mathrm{r,d}})/(\kappa_{\mathrm{r}} + \kappa_{\mathrm{r,d}})$.

IV. PURCELL RATE WITH MICROWAVE DRIVE AND BANDPASS FILTER

The Purcell rate may decrease when the measurement microwave drive is added [23]. A simple physical reason is the ac Stark shift, which in the typical setup increases the absolute value of detuning between the qubit and readout resonator with increasing number of photons in the resonator, thus reducing the Purcell rate. However, this explanation may not necessarily work well quantitatively.

The Purcell rate suppression due to the microwave drive was analyzed in Ref. [23] for the case without the Purcell filter and using the two-level approximation for the qubit. It was shown that in this case the suppression factor $\Gamma(\bar{n})/\Gamma(0)$ is approximately $[(1 + \bar{n}/n_{\mathrm{crit}})^{-1/2} + (1 + \bar{n}/n_{\mathrm{crit}})^{-1}]^2$ instead of the factor $(1 + \bar{n}/n_{\mathrm{crit}})^{-1}$ expected from the ac Stark shift, where $\bar{n}$ is the mean number of photons in the resonator and $n_{\mathrm{crit}} \equiv (\Delta_{\mathrm{rq}}/2g)^2$. This difference results in the ratio 3/2 between the corresponding slopes of $\Gamma(\bar{n})$ at small $\bar{n}$, with the ac Stark shift model underestimating the Purcell rate suppression (see the blue lines in Fig. 4). However, when the third level of the qubit is taken into account, then the ac Stark

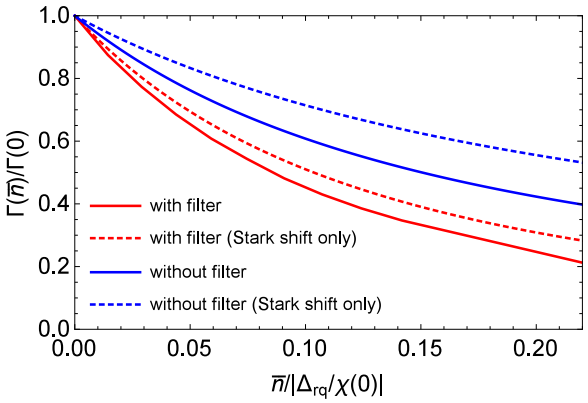

FIG. 4. (Color online) The Purcell relaxation rate $\Gamma(\bar{n})$ with a microwave drive, normalized by the no-drive rate $\Gamma(0)$, with the filter (red solid curve) and without the filter (blue solid curve), as functions of the mean number of photons $\bar{n}$ in the readout resonator. The numerical simulations used the two-level approximation for the qubit, for which $\bar{n}/|\Delta_{\rm rq}/\chi(0)| = \bar{n}/4n_{\rm crit}$. The dashed lines show the values expected from the model based on the ac Stark shift: $\Gamma(\bar{n})/\Gamma(0) = (1+\bar{n}/n_{\rm crit})^{-2}$ with the filter and $(1+\bar{n}/n_{\rm crit})^{-1}$ without the filter. The parameters used in the simulations are given in the text.

shift model describes correctly the slope of $\Gamma(\bar{n})$ at small $\bar{n}$ when the qubit anharmonicity is relatively small, $|\delta_{\rm q}/\Delta_{\rm rq}| \ll 1$ (see Appendix). In this case the ac Stark shift model predicts $\Gamma(\bar{n})/\Gamma(0) = 1 + 4\bar{n}\chi(0)/\Delta_{\rm rq}$ at $\bar{n} \ll n_{\rm crit}$, where $\chi(0)$ is the value of χ at $\bar{n} = 0$; note that $|\chi(0)| \ll |g^2/\Delta_{\rm rq}|$ and $\chi(0) < 0$ when $\Delta_{\rm rq} > 0$.

With the filter resonator, we also expect that the ac Stark shift model for the Purcell rate suppression should work reasonably well, so that from Eq. (32) we expect

$$\Gamma(\bar{n}) \approx \frac{g^2|\mathcal{G}|^2\kappa_{\rm f}}{[\omega_{\rm r} - \omega_{\rm q,eff}(\bar{n})]^2\{[\omega_{\rm f} - \omega_{\rm q,eff}(\bar{n})]^2 + (\kappa_{\rm f}/2)^2\}}, \quad (44)$$

where $\omega_{\rm q,eff}(\bar{n})$ is the effective qubit frequency, $\omega_{\rm q,eff}(\bar{n}) = \omega_{\rm q}^{\rm b} + 2\chi(0)\bar{n}$ if we neglect dependence of χ on $\bar{n}$ and the "Lamb shift." Therefore, in a typical situation when $|\omega_{\rm f} - \omega_{\rm r}| \ll |\omega_{\rm r} - \omega_{\rm q}|$ and $\kappa_{\rm f} \ll |\omega_{\rm r} - \omega_{\rm q}|$, we expect the suppression ratio

$$\frac{\Gamma(\bar{n})}{\Gamma(0)} \approx \left[\frac{\omega_{\rm r} - \omega_{\rm q}^{\rm b}}{\omega_{\rm r} - \omega_{\rm q,eff}(\bar{n})}\right]^4. \quad (45)$$

To check the accuracy of this formula numerically, we need to add into the Hamiltonian (22) the terms describing the drive and higher levels in the qubit (see Appendix). However, the resulting Hilbert space was too large for our numerical simulations, so we numerically calculated $\Gamma(\bar{n})$ using only the two-level approximation for the qubit. Using the rotating frame based on the drive frequency $\omega_{\rm d}$ [i.e., $H_0 = \omega_{\rm d}(\sigma_+\sigma_- + a^\dagger a + b^\dagger b)$], we then obtain the interaction Hamiltonian

$$V_{\rm d} = \Delta_{\rm rd}a^\dagger a + \Delta_{\rm fd}b^\dagger b + \Delta_{\rm qd}\sigma_+\sigma_- + g(a^\dagger\sigma_- + a\sigma_+) + \mathcal{G}a^\dagger b + \mathcal{G}^* a b^\dagger + \varepsilon_{\rm r}a^\dagger + \varepsilon_{\rm r}^* a, \quad (46)$$

where $\Delta_{\rm rd} = \omega_{\rm r}^{\rm b} - \omega_{\rm d}$, $\Delta_{\rm fd} = \omega_{\rm f} - \omega_{\rm d}$, $\Delta_{\rm qd} = \omega_{\rm q}^{\rm b} - \omega_{\rm d}$, and for simplicity we assumed that the drive $\varepsilon_{\rm r}$ is applied to the readout resonator. (For the rotating wave approximation we also need to assume that $|\Delta_{\rm rd}|$, $|\Delta_{\rm fd}|$, $|\Delta_{\rm qd}|$, $|g|$, $|\mathcal{G}|$, and $|\dot{\varepsilon}_{\rm r}/\varepsilon_{\rm r}|$ are all small compared with $\omega_{\rm d}$.) Note that in the two-level approximation $[\omega_{\rm r} - \omega_{\rm q,eff}(\bar{n})]^2 = \Delta_{\rm rq}^2 + 4g^2\bar{n} = \Delta_{\rm rq}^2(1 + \bar{n}/n_{\rm crit})$.

We have numerically solved the full master equation with the Hamiltonian (23), including the decay $\kappa_{\rm f}$ of the filter resonator. As the initial state we use the excited state for the qubit and vacuum for the two resonators, $|\psi\rangle_{\rm in} = |{\rm e}00\rangle$. The Purcell rate is extracted from the numerical solution of $\rho_{ee}(t)$ by fitting $-\ln[\rho_{ee}(t)]$ with a linear function in the long time limit [still requiring $1 - \rho_{ee}(t) \ll 1$]. In the simulations we pump the readout resonator with the frequency $\omega_{\rm d} = \omega_{\rm r}^{|e\rangle}$ and control $\bar{n}$ by choosing the corresponding value of $\varepsilon_{\rm r}$. The value of $\bar{n}$ is calculated numerically; it is close to what is expected from the solution of the classical field equations when the n dependence of χ and $\omega_{\rm r}^{|e\rangle}$ is taken into account: in the two-level approximation $\chi(\bar{n}) = -g^2/[\Delta_{\rm rq}\sqrt{1 + 4g^2\bar{n}/\Delta_{\rm rq}^2}]$ and $\omega_{\rm r}^{|e\rangle} = \omega_{\rm r}^{\rm b} + \chi(\bar{n})$. Since $\omega_{\rm r}^{|e\rangle}$ changes with $\bar{n}$, we change $\omega_{\rm d}$ accordingly.

The red solid line in Fig. 4 shows the numerical results for the Purcell rate suppression factor $\Gamma(\bar{n})/\Gamma(0)$ as a function of $\bar{n} = \bar{n}^{|e\rangle}$, normalized by $|\Delta_{\rm rq}/\chi(0)|$. Note that in the two-level approximation (which we used in the simulations) $\bar{n}/|\Delta_{\rm rq}/\chi(0)| = \bar{n}/4n_{\rm crit}$. In the simulations we have used $g/2\pi = 100\,{\rm MHz}$, $\kappa_{\rm r}^{-1} = 36\,{\rm ns}$, $\kappa_{\rm f}^{-1} = 0.71\,{\rm ns}$, $\omega_{\rm r}^{\rm b}/2\pi = \omega_{\rm f}/2\pi = 6.8\,{\rm GHz}$, and $\omega_{\rm q}^{\rm b}/2\pi = 6\,{\rm GHz}$. The blue solid line shows the numerical suppression factor for the standard setup [23] (without the filter resonator), also in the two-level approximation for the qubit. We see a larger suppression for the case with the filter, as expected from the ac Stark shift interpretation and the fact that $\Gamma \propto \Delta_{\rm rq}^{-4}$ with the filter, while $\Gamma \propto \Delta_{\rm rq}^{-2}$ in the standard setup. However, comparison with the prediction of the ac Stark shift model (dashed lines) does not show a quantitative agreement. There is about 10% discrepancy for the slope of $\Gamma(\bar{n})$ between the red solid and red dashed lines in the case with the filter. This is a better agreement than for the case without the filter (blue lines).

Note that the numerical calculations have been made using only the two-level model for the qubit. It is possible that the agreement between the ac Stark shift model and the numerical results is much better if three or more levels in the qubit are taken into account. This is an interesting question for further research.

Also note that in experiments, increase of the drive power often leads to decrease of the qubit lifetime, instead of the increase, predicted by our analysis (both with and without the filter). The reason for this effect is not quite clear and may be related to various technical issues. Therefore, either suppression or enhancement of the qubit relaxation with the drive power may be observed in actual experiments.

V. CONCLUSION

In this paper we have discussed the theory of the bandpass Purcell filter used in Refs. [10,17] for measurement of

superconducting qubits. An additional wide-bandwidth filter resonator (Fig. 2) coupled to the readout resonator easily passes the microwave field used for the qubit measurement, but strongly impedes the propagation of a photon at the qubit frequency, which is far outside of the filter bandwidth. A simple way to quantitatively describe the operation of the filter is by noticing that the effective decay rate $\kappa_{\rm eff}$ of the readout resonator [Eq. (8)] depends on frequency. Therefore, the measurement is governed by a relatively large value $\kappa_{\rm r}$ [Eq. (10)], which permits a fast measurement, while the Purcell relaxation is determined by a much smaller value $\kappa_{\rm q}$ seen by the qubit [Eq. (11)]. The ratio of these effective decay rates of the readout resonator gives the suppression factor for the qubit relaxation [Eq. (12)]. The result for the suppression factor is similar to the result obtained in Ref. [17] using circuit theory (with a few minor differences).

We have first analyzed the operation of the Purcell filter quasiclassically, and then confirmed the results using the quantum approach. In the quantum analysis we have used two approaches: based on decaying wave function and density matrix evolutions. While the Purcell effect is traditionally described using density matrices, it is actually simpler to use the approach based on wave functions. The results of our semiclassical and two quantum approaches are very close to each other; however, they are not identical because the approaches use slightly different approximations. A simple and most physically transparent result for the Purcell rate is given by Eq. (32).

The Purcell rate of the qubit decay is further suppressed when a microwave drive is applied for measurement. The effect is similar to what was discussed in Ref. [23] for the standard setup without the filter, and can be crudely understood as being due to the ac Stark shift of the qubit frequency, which increases the resonator-qubit detuning $\Delta_{\rm rq}$. Since the Purcell rate with the filter scales with $\Delta_{\rm rq}$ crudely as $\Delta_{\rm rq}^{-4}$ [Eq. (32)] instead of $\Delta_{\rm rq}^{-2}$ in the standard setup, the Purcell rate suppression due to microwaves is stronger in the case with the filter. Numerical results for the suppression due to microwaves using the two-level approximation for the qubit show that the explanation based on ac Stark shift works well, but underestimates the effect by about 10%. This discrepancy may be significantly less if more levels in the qubit are taken into account; however, this still remains an open question.

The bandpass Purcell filter decreases the qubit decay due to the Purcell effect by a factor of ∼50 for typical parameters, for the same measurement conditions as in the standard setup without the filter. This allows much faster and more accurate measurement of superconducting qubits, compared to the case without the filter. The qubit measurement within 140 ns with 99% fidelity using this filter has been demonstrated in Ref. [17]. With a slight change of parameters it seems possible to perform qubit readout within ∼50 ns with fidelity approaching 99.9%. Such fast and accurate qubit readout would be very useful for quantum information processing with superconducting qubits.

ACKNOWLEDGMENTS

The authors thank Daniel Sank, Mostafa Khezri, and Justin Dressel for useful discussions. The research was funded by the Office of the Director of National Intelligence (ODNI), Intelligence Advanced Research Projects Activity (IARPA), through the Army Research Office Grant No. W911NF-10-1-0334. All statements of fact, opinion or conclusions contained herein are those of the authors and should not be construed as representing the official views or policies of IARPA, the ODNI, or the U.S. Government. We also acknowledge support from the ARO MURI Grant No. W911NF-11-1-0268.

APPENDIX: QUBIT MEASUREMENT AND PURCELL EFFECT IN THE STANDARD SETUP

In this Appendix we review the trade-off between the Purcell rate and measurement time for a transmon or Xmon qubit in the standard cQED setup (without a filter). In the standard setup [11,12,24] (Fig. 1) the qubit is dispersively coupled with the resonator, so that the qubit state slightly changes the resonator frequency. This change causes a phase shift (and in general an amplitude change) of a microwave field transmitted through or reflected from the resonator. The transmitted or reflected microwave is then amplified and sent to a mixer, so that the phase shift (and amplitude change) can be discriminated, thus distinguishing the states $|g\rangle$ and $|e\rangle$ of the qubit.

1. Basic theory

For the basic analysis of measurement [24], it is sufficient to consider *three* energy levels of the qubit: the ground state $|g\rangle$, the first excited state $|e\rangle$, and the second excited state $|f\rangle$, so that the Hamiltonian is ($\hbar = 1$)

$$\begin{aligned} H = {} & \omega_{\rm q}^{\rm b}|e\rangle\langle e| + \left(2\omega_{\rm q}^{\rm b} - \delta_{\rm q}\right)|f\rangle\langle f| + \omega_{\rm r}^{\rm b} a^\dagger a \\ & + g a^\dagger |g\rangle\langle e| + g^* a|g\rangle\langle e| + \tilde{g} a^\dagger |e\rangle\langle f| + \tilde{g}^* a|f\rangle\langle e| \\ & + \varepsilon_{\rm r} a^\dagger e^{-i\omega_{\rm d} t} + \varepsilon_{\rm r}^* a e^{i\omega_{\rm d} t} + H_\kappa + H_\gamma, \end{aligned} \tag{A1}$$

where $\omega_{\rm q}^{\rm b}$ is the bare qubit frequency, $\delta_{\rm q}$ is its anharmonicity ($\delta_{\rm q} > 0$, $\delta_{\rm q}/\omega_{\rm q}^{\rm b} \sim 0.2\,{\rm GHz}/6\,{\rm GHz} \ll 1$), $\omega_{\rm r}^{\rm b}$ is the bare resonator frequency, a is the annihilation operator for the resonator, g is the coupling between the qubit and the resonator, $\tilde{g} \approx \sqrt{2}\, g$ is the similar coupling involving levels $|e\rangle$ and $|f\rangle$, and $\varepsilon_{\rm r}$ is the normalized amplitude of the microwave drive with frequency $\omega_{\rm d}$. For brevity H_κ describes the coupling of the resonator with the transmission line, which causes resonator energy damping with the rate κ, while H_γ describes the intrinsic qubit relaxation (excluding the Purcell effect) with the rate $T_{1,\rm int}^{-1}$. Note that in the Hamiltonian (A1) we neglected the coupling terms creating or annihilating the double excitations in the qubit and the resonator. For simplicity we assume a real coupling: $g^* = g$ and $\tilde{g}^* = \tilde{g}$.

For a simple analysis of the measurement process, let us first neglect H_κ, H_γ, and the drive ε_r, and consider the three Jaynes-Cummings ladders of states $|g,n\rangle$, $|e,n\rangle$, and $|f,n\rangle$, where n denotes the number of photons in the resonator. The coupling g provides the level repulsion between $|g,n+1\rangle$ and $|e,n\rangle$ (effective coupling is $\sqrt{n+1}\, g$), while $\tilde{g}$ provides the level repulsion between $|e,n+1\rangle$ and $|f,n\rangle$ (with coupling $\sqrt{n+1}\, \tilde{g}$). Assuming sufficiently large level separation, $|\omega_{\rm q}^{\rm b} - \omega_{\rm r}^{\rm b}| \gg \sqrt{n}\,|g|$ and $|\omega_{\rm q}^{\rm b} - \delta_{\rm q} - \omega_{\rm r}^{\rm b}| \gg \sqrt{n}\,|\tilde{g}|$, we can treat the level repulsion to lowest order; then the energies of the

eigenstates $\overline{|g,n\rangle}$ and $\overline{|e,n\rangle}$ are

$$E_{\overline{|g,n\rangle}} = n\omega_{\rm r}^{\rm b} - \frac{ng^2}{\omega_{\rm q}^{\rm b} - \omega_{\rm r}^{\rm b}}, \tag{A2}$$

$$E_{\overline{|e,n\rangle}} = \omega_{\rm q}^{\rm b} + n\omega_{\rm r}^{\rm b} + \frac{(n+1)\,g^2}{\omega_{\rm q}^{\rm b} - \omega_{\rm r}^{\rm b}} - \frac{n\tilde{g}^2}{\omega_{\rm q}^{\rm b} - \delta_{\rm q} - \omega_{\rm r}^{\rm b}}. \tag{A3}$$

Therefore, the effective resonator frequency $\omega_{\rm r}^{|g\rangle}$ when the qubit in the ground state is

$$\omega_{\rm r}^{|g\rangle} = E_{\overline{|g,n+1\rangle}} - E_{\overline{|g,n\rangle}} = \omega_{\rm r}^{\rm b} - \frac{g^2}{\Delta}, \tag{A4}$$

where

$$\Delta = \Delta_{\rm qr} = \omega_{\rm q}^{\rm b} - \omega_{\rm r}^{\rm b}, \tag{A5}$$

while for the qubit state $|e\rangle$ the effective resonator frequency is

$$\omega_{\rm r}^{|e\rangle} = E_{\overline{|e,n+1\rangle}} - E_{\overline{|e,n\rangle}} = \omega_{\rm r}^{\rm b} + \frac{g^2}{\Delta} - \frac{\tilde{g}^2}{\Delta - \delta_{\rm q}}. \tag{A6}$$

Denoting the frequency difference by 2χ, we obtain

$$\omega_{\rm r}^{|e\rangle} - \omega_{\rm r}^{|g\rangle} = 2\chi, \tag{A7}$$

$$\chi = \frac{g^2}{\Delta} - \frac{\tilde{g}^2/2}{\Delta - \delta_{\rm q}} = -\frac{g^2\delta_{\rm q}}{\Delta(\Delta - \delta_{\rm q})} + \frac{g^2 - \tilde{g}^2/2}{\Delta - \delta_{\rm q}}. \tag{A8}$$

The corresponding effective qubit frequency is

$$\omega_{\rm q}^{\rm eff} = E_{\overline{|e,n\rangle}} - E_{\overline{|g,n\rangle}} = \omega_{\rm q}^{\rm b} + \frac{g^2}{\Delta} + 2n\chi, \tag{A9}$$

which includes the "Lamb shift" g^2/Δ and the "ac Stark shift" $2n\chi$.

Therefore, in this case the first two lines of the Hamiltonian (A1) can be approximated as

$$H = \frac{\omega_{\rm q}}{2}\,\sigma_z + \omega_{\rm r} a^\dagger a + \chi a^\dagger a\,\sigma_z, \tag{A10}$$

where

$$\omega_{\rm q} = \omega_{\rm q}^{\rm b} + \frac{g^2}{\Delta}, \quad \omega_{\rm r} = \omega_{\rm r}^{\rm b} - \frac{1}{2}\,\frac{\tilde{g}^2}{\Delta - \delta_{\rm q}}, \tag{A11}$$

$\sigma_z = |e\rangle\langle e| - |g\rangle\langle g|$, we shifted the energy by $-\omega_{\rm q}/2$, and we no longer need the qubit state $|f\rangle$.

Note that the dispersive coupling χ given by Eq. (A8) is much smaller [24] than the value g^2/Δ expected in the two-level case. This is because the transmon and Xmon qubits are only slightly different from a linear oscillator, for which $\tilde{g} = \sqrt{2}\,g$ and $\delta_{\rm q} = 0$, thus leading to $\chi = 0$. The effect of nonzero anharmonicity $\delta_{\rm q}$ in Eq. (A8) is more important than the effect of nonzero $\tilde{g} - \sqrt{2}\,g$ because

$$\frac{\tilde{g}^2}{2} - g^2 \approx -g^2\frac{\delta_{\rm q}}{\omega_{\rm q}^{\rm b}} \tag{A12}$$

and $|\Delta| \ll \omega_{\rm q}^{\rm b}$. Therefore, χ can be approximated as

$$\chi \approx -\frac{g^2\delta_{\rm q}}{\Delta(\Delta - \delta_{\rm q})} \approx -\frac{g^2\delta_{\rm q}}{\Delta^2}, \tag{A13}$$

where the last formula also assumes $|\Delta| \gg \delta_{\rm q}$.

The dispersive approximation (A10) is based on the approximate formulas (A2) and (A3) for the eigenenergies, and therefore requires a limited number of photons n in the resonator,

$$n \ll \min(n_{\rm crit}, \tilde{n}_{\rm crit}), \quad n_{\rm crit} = \frac{\Delta^2}{4g^2}, \quad \tilde{n}_{\rm crit} = \frac{(\Delta - \delta_{\rm q})^2}{4\tilde{g}^2}, \tag{A14}$$

where the factor 4 in the definitions of the critical photon numbers $n_{\rm crit}$ and $\tilde{n}_{\rm crit}$ is a usual convention. For n beyond this range it is still possible (at least to some extent) to use the dispersive approximation (A10) if the spread of n is relatively small; however $\omega_{\rm q}$, $\omega_{\rm r}$, and χ should be redefined. For that we need to use similar steps as in Eqs. (A4)–(A9), but starting with more accurate formulas than (A2) and (A3). In particular, in the two-level approximation for the qubit ($\tilde{g} = 0$ or $\delta_{\rm q} = \infty$) we would obtain $\chi \approx g^2/\sqrt{\Delta^2 + 4\bar{n}g^2}$ with $\bar{n}$ being the average (typical) number of photons; however, the generalization of the realistic case (A13) is not so simple (see below).

The dispersive approximation (A10) cannot reproduce the Purcell effect [11] after including the last line of the Hamiltonian (A1), so it should be added separately. Without the microwave drive ($\varepsilon_{\rm r} = 0$) only levels $|e,0\rangle$, $|g,1\rangle$, and $|g,0\rangle$ are involved into the evolution described by Eq. (A1), and for sufficiently small resonator bandwidth, $\kappa \ll \sqrt{\Delta^2 + 4g^2}$, the qubit relaxation rate due to Purcell effect is

$$\Gamma \approx \frac{\kappa}{2}\left(1 - \frac{|\Delta|}{\sqrt{\Delta^2 + 4g^2}}\right) \approx \frac{g^2\kappa}{\Delta^2}. \tag{A15}$$

Note that this rate does not depend on the qubit anharmonicity $\delta_{\rm q}$, in contrast to the dispersive coupling χ, which vanishes at $\delta_{\rm q} \to 0$. This is because the *Purcell effect is essentially a linear effect* (energy decay via decay of a coupled system), in contrast to χ, which is based on qubit nonlinearity. This linearity is the reason why the Purcell rate Γ does not change (in the first approximation) when the microwave drive $\varepsilon_{\rm r}$ creates a significant photon population in the resonator, $1 \ll n \ll \min(n_{\rm crit}, \tilde{n}_{\rm crit})$. (Someone might naively expect that Γ scales with n because of effective coupling $\sqrt{n}\,g$.) However, in the next approximation Γ depends on n [23] and can be calculated as

$$\Gamma(n) = \kappa\,|\overline{\langle g,n|}a\overline{|e,n\rangle}|^2, \tag{A16}$$

with subsequent replacement of n with the average photon number $\bar{n}$ if the spread of n is relatively small.

Using the third-order (in g and/or $\tilde{g}$) eigenstates,

$$\begin{aligned}\overline{|g,n\rangle} = {} & \left(1 - \frac{ng^2}{2\Delta^2}\right)|g,n\rangle + \frac{\sqrt{n(n-1)}\,g\tilde{g}}{\Delta(2\Delta - \delta_{\rm q})}\,|f,n-2\rangle \\ & - \frac{\sqrt{n}\,g}{\Delta}\left(1 - \frac{3ng^2}{2\Delta^2} + \frac{(n-1)\tilde{g}^2}{\Delta(2\Delta - \delta_{\rm q})}\right)|e,n-1\rangle,\end{aligned} \tag{A17}$$

$$\begin{aligned}\overline{|e,n\rangle} \approx {} & \left(1 - \frac{(n+1)g^2}{2\Delta^2} - \frac{n\tilde{g}^2}{2(\Delta - \delta_{\rm q})^2}\right)|e,n\rangle \\ & + \frac{\sqrt{n+1}\,g}{\Delta}\left(1 - \frac{3(n+1)g^2}{2\Delta^2} + \frac{n\tilde{g}^2(\Delta - 2\delta_{\rm q})}{2\Delta(\Delta - \delta_{\rm q})^2}\right) \\ & \times|g,n+1\rangle - \frac{\sqrt{n}\,\tilde{g}}{\Delta - \delta_{\rm q}}\,|f,n-1\rangle,\end{aligned} \tag{A18}$$

where the last term in Eq. (A18) for brevity is only of the first order, we find the Purcell rate

$$\Gamma(n) = \kappa \frac{g^2}{\Delta^2}\left(1 - \frac{3g^2}{\Delta^2} - 6n\frac{g^2}{\Delta^2} + n\frac{\tilde{g}^2(3\Delta - 4\delta_q)}{\Delta(\Delta-\delta_q)^2}\right), \quad \text{(A19)}$$

which is an approximation up to fifth order in g. This result coincides with the result of Ref. [23] when $\tilde{g} = 0$. Approximating $\tilde{g} = \sqrt{2}\,g$ [see Eq. (A12)], we obtain

$$\Gamma(n) \approx \kappa \frac{g^2}{\Delta^2}\left(1 - \frac{3g^2}{\Delta^2} + n\,\frac{2g^2\delta_q(2\Delta - 3\delta_q)}{\Delta^2(\Delta-\delta_q)^2}\right). \quad \text{(A20)}$$

It is interesting to note that while in the two-level approximation ($\tilde{g} = 0$) the Purcell rate is always suppressed with increasing n [23], Eq. (A20) shows the suppression only when $\Delta < (3/2)\delta_q$ (which is the usual experimental case, since Δ is usually negative). Numerical results using Eq. (A16) show that even when $\Gamma(n)$ initially increases with n, it is still suppressed at larger n. Note that the result (A20) requires assumption (A14) of a sufficiently small nonlinearity. Comparing Eqs. (A20) and (A13), we see that in the case of large detuning, $|\Delta| \gg \delta_q$, the dependence of the Purcell rate on n is consistent with the explanation based on the ac Stark shift, $\Gamma(n) \approx \kappa g^2/(\Delta + 2n\chi)^2$. (This is in contrast to the two-level approximation, in which this explanation leads to a discrepancy in the slope [23] by a factor of 3/2.) We have checked that taking into account the fourth level in the qubit does not change Eqs. (A19) and (A20); there are no additional contributions of the order g^4.

Besides the qubit energy relaxation Γ, the resonator damping κ in the presence of drive leads to the qubit excitation [23] $|g\rangle \to |e\rangle$ with the rate $\Gamma_{|g\rangle\to|e\rangle} = \kappa\,|\overline{\langle e,n-2|}a|\overline{g,n\rangle}|^2$ and the excitation $|e\rangle \to |f\rangle$ with the rate $\Gamma_{|e\rangle\to|f\rangle} = \kappa\,|\overline{\langle f,n-2|}a|\overline{e,n\rangle}|^2$. These rates (up to sixth order in coupling) are

$$\Gamma_{|g\rangle\to|e\rangle} = \frac{\kappa g^2 n(n-1)}{\Delta^2}\left[\frac{g^2}{\Delta^2} - \frac{\tilde{g}^2}{\Delta(2\Delta-\delta_q)}\right]^2 \quad \text{(A21)}$$

$$\approx \frac{\kappa g^2}{\Delta^2}\left(\frac{n}{n_{\rm crit}}\right)^2 \frac{\delta_q^2}{16\,(2\Delta-\delta_q)^2}, \quad \text{(A22)}$$

$$\Gamma_{|e\rangle\to|f\rangle} = \frac{\kappa \tilde{g}^2 n(n-1)}{(\Delta-\delta_q)^4}\left[\frac{\tilde{g}^2}{\Delta-\delta_q} - \frac{g^2}{2\Delta-\delta_q} - \frac{\tilde{\tilde{g}}^2}{2\Delta-3\delta_q}\right]^2 \quad \text{(A23)}$$

$$\approx \frac{\kappa g^2}{\Delta^2}\,\frac{(n/n_{\rm crit})^2\,\delta_q^2\Delta^8}{2(\Delta-\delta_q)^6(2\Delta-\delta_q)^2(2\Delta-3\delta_q)^2}, \quad \text{(A24)}$$

where $\tilde{\tilde{g}} \approx \sqrt{3}\,g$ is the coupling due to the fourth qubit level with energy $3\omega_q^b - 3\delta_q$, and in Eqs. (A22) and (A24) we also used $\tilde{g} = \sqrt{2}\,g$ and replaced $n(n-1)$ with n^2. In the assumed range, $n \ll n_{\rm crit}$, the excitation rates are much smaller than the Purcell decay rate Γ.

Now let us discuss the n dependence of the dispersive coupling $\chi(n) = [\omega_r^{|e\rangle}(n) - \omega_r^{|g\rangle}(n)]/2$, where $\omega_r^{|g\rangle}(n) = E_{\overline{|g,n+1\rangle}} - E_{\overline{|g,n\rangle}}$ and $\omega_r^{|e\rangle}(n) = E_{\overline{|e,n+1\rangle}} - E_{\overline{|e,n\rangle}}$ [see Eqs. (A4), (A6), and (A7)]. Using the three-level approximation for the qubit with accuracy up to the fourth order in g and/or $\tilde{g}$ (assuming $n \ll n_{\rm crit}$), we obtain

$$\omega_r^{|g\rangle}(n) = -\frac{g^2}{\Delta} + \frac{g^4(2n+1)}{\Delta^3} - \frac{2g^2\tilde{g}^2 n}{\Delta^2(2\Delta-\delta_q)}, \quad \text{(A25)}$$

$$\omega_r^{|e\rangle}(n) = \frac{g^2}{\Delta} - \frac{\tilde{g}^2}{\Delta-\delta_q} - \frac{g^4(2n+3)}{\Delta^3} + \frac{\tilde{g}^4(2n+1)}{(\Delta-\delta_q)^3} - \frac{2\delta_q g^2\tilde{g}^2(n+1)}{\Delta^2(\Delta-\delta_q)^2}, \quad \text{(A26)}$$

so that assuming $\tilde{g} = \sqrt{2}\,g$, we obtain

$$\chi(n) \approx -\frac{g^2\delta_q}{\Delta(\Delta-\delta_q)} + \frac{4g^4\delta_q}{\Delta^4}\,\frac{1-\tilde{\delta}_q+\tilde{\delta}_q^2/2}{(1-\tilde{\delta}_q)^3} + \frac{3ng^4}{\Delta^3}\,\frac{1-\tilde{\delta}_q^2+\tilde{\delta}_q^3-\tilde{\delta}_q^4/3}{(1-\tilde{\delta}_q/2)(1-\tilde{\delta}_q)^3}, \quad \text{(A27)}$$

where $\tilde{\delta}_q = \delta_q/\Delta$. This result predicts a quite strong n dependence of χ, which is, however, not correct. The reason is that it is not sufficient to consider three qubit levels for $\chi(n)$. When the fourth level of the qubit is taken into account (with energy $3\omega_q^b - 3\delta_q$ and coupling $\tilde{\tilde{g}}$), this does not change Eq. (A25) for $\omega_r^{|g\rangle}(n)$, but introduces an additional term

$$-\frac{2\tilde{g}^2\tilde{\tilde{g}}^2 n}{(\Delta-\delta_q)^2(2\Delta-3\delta_q)} \quad \text{(A28)}$$

into Eq. (A26) for $\omega_r^{|e\rangle}(n)$. Assuming $\tilde{\tilde{g}} = \sqrt{3}\,g$, this changes Eq. (A27) into

$$\chi(n) \approx -\frac{g^2\delta_q}{\Delta(\Delta-\delta_q)} + \frac{4g^4\delta_q}{\Delta^4}\,\frac{1-\tilde{\delta}_q+\tilde{\delta}_q^2/2}{(1-\tilde{\delta}_q)^3} - \frac{9ng^4\delta_q^2}{2\Delta^5}\,\frac{1-(5/3)\tilde{\delta}_q+(11/9)\tilde{\delta}_q^2-\tilde{\delta}_q^3/3}{(1-\tilde{\delta}_q/2)(1-\tilde{\delta}_q)^3(1-3\tilde{\delta}_q/2)}. \quad \text{(A29)}$$

which shows a quite weak dependence on n,

$$\frac{d\chi(n)}{dn} \approx \frac{9}{8}\,\frac{\delta_q}{\Delta}\,\frac{\chi(0)}{n_{\rm crit}}, \quad \text{(A30)}$$

assuming $\delta_q \ll |\Delta|$. In the usual case when $\Delta < 0$, the absolute value of $\chi(n)$ decreases with increasing n.

Note that in Eqs. (A27) and (A29) we used $\tilde{g} = \sqrt{2}\,g$ and $\tilde{\tilde{g}} = \sqrt{3}\,g$. If a better approximation is used,

$$\tilde{g} \approx \sqrt{2}\,g\,(1 - \delta_q/2\omega_q^b), \quad \tilde{\tilde{g}} \approx \sqrt{3}\,g\,(1-\delta_q/\omega_q^b), \quad \text{(A31)}$$

then correction to the $\tilde{g}^2$ term in Eq. (A26) creates an additional contribution $g^2\delta_q/[\omega_q^b(\Delta-\delta_q)]$ to χ, which for typical parameters is much larger than the second terms in Eqs. (A27) and (A29). The correction (A31) also yields an additional n-dependent contribution of approximately $2g^4\delta_q n/(\Delta^3\omega_q^b)$ (assuming $\delta_q \ll |\Delta|$) to both $\omega_r^{|g\rangle}(n)$ and $\omega_r^{|e\rangle}(n)$. These additional slopes are comparable to the slope of $\chi(n)$ in Eq. (A29) because $\Delta^2/(\delta_q\omega_q^b)$ is on the order of 1 for typical experimental parameters. However, the contribution to $\chi(n)$ from the correction (A31) is only $9g^4\delta_q^2 n/(\Delta^4\omega_q^b)$ (assuming $\delta_q \ll |\Delta|$), which is smaller than the last term in Eq. (A29) because $|\Delta| \ll \omega_q^b$. Therefore, the slope of $\chi(n)$ in Eq. (A29) is practically not affected by the correction (A31).

Similarly, inaccuracy of our approximation of the fourth qubit level energy by $3\omega_q^b - 3\delta_q$ produces only a small correction to the slope of $\chi(n)$: the correction to the fourth-level energy is on the order of δ_q^2/ω_q^b, and therefore the correction to $\chi(n)$ [via Eq. (A28)] is on the order of $g^4\delta_q^2 n/(\Delta^4\omega_q^b)$ for $\delta_q \ll |\Delta|$.

Thus, we see that for a transmon or Xmon qubit, calculation of $\chi(0)$ requires at least three qubit levels to be taken into account, while the first correction due to $\chi(n)$ dependence ($n \ll n_{crit}$) requires at least four qubit levels to be considered. In contrast, calculation of the Purcell rate $\Gamma(0)$ requires two qubit levels, while the first correction due to $\Gamma(n)$ dependence requires three qubit levels.

2. Measurement error

Now let us discuss the qubit measurement error caused by the qubit relaxation due to Purcell effect. To describe measurement, we will use the dispersive approximation (A10) with $\chi = -g^2\delta_q/\Delta^2$ [Eq. (A13)] and neglect the small difference between Δ defined in Eq. (A5) and $\omega_q - \omega_r$ defined via Eq. (A11). For the Purcell rate we will use the simplest form $\Gamma = g^2\kappa/\Delta^2$. Both approximations assume a sufficiently small number of photons, Eq. (A14).

Assuming that the qubit is either in the state $|g\rangle$ or $|e\rangle$ (nonevolving), from Eq. (A10) we see that the effective resonator frequency is constant in time, $\omega_r \pm \chi$, where the upper sign is for the state $|e\rangle$ and the lower sign is for $|g\rangle$. The corresponding resonator state is a coherent state $|\alpha_\pm\rangle$, characterized by an amplitude $\alpha_\pm(t)$ in the rotating frame based on the drive frequency ω_d [in the laboratory frame the resonator wave function is $e^{-|\alpha_\pm|^2/2}\sum_n(\alpha_\pm e^{-i\omega_d t})^n n^{-1/2}|n\rangle$ up to an overall phase]. The evolution of the amplitude is

$$\dot\alpha_\pm = -i(\Delta_{rd} \pm \chi)\,\alpha_\pm - \frac{\kappa}{2}\,\alpha_\pm - i\varepsilon_r, \tag{A32}$$

where the upper sign everywhere is for the state $|e\rangle$,

$$\Delta_{rd} = \omega_r - \omega_d, \tag{A33}$$

and complex $\varepsilon_r(t)$ can in general depend on time to describe a drive with changing amplitude and frequency. (Note a difference in notation compared with the main text: now Δ_{rd} does not depend on the qubit state and the frequency shift $\pm\chi$ is added explicitly.) The steady state for a steady drive, $\varepsilon_r = \text{const}$, is

$$\alpha_\pm = \frac{-i\varepsilon_r}{\kappa/2 + i(\Delta_{rd} \pm \chi)}, \tag{A34}$$

so that the two coherent states are separated by

$$\alpha_+ - \alpha_- = \frac{-2\varepsilon_r\chi}{(\kappa/2 + i\,\Delta_{rd})^2 + \chi^2}, \tag{A35}$$

and this is the difference, which can be sensed by the homodyne detection (it does not matter whether the microwave is transmitted or reflected from the resonator when we discuss the measurement in terms of $\alpha_\pm$).

In the case when $\Delta_{rd} = 0$ (so that $\omega_d = \omega_r$), both states have the same average number of photons, $\bar n = |\alpha_+|^2 = |\alpha_-|^2 = |\varepsilon_r|^2/(\kappa^2/4 + \chi^2)$, and the absolute value of the state separation is

$$\delta\alpha \equiv |\alpha_+ - \alpha_-| = \frac{2\sqrt{\bar n}}{\sqrt{(\kappa/2\chi)^2 + 1}}. \tag{A36}$$

Theoretically, the distinguishability of two coherent states separated by $\delta\alpha$ is the same as the distinguishability of two Gaussians with width (standard deviation) of $1/2$ each, separated by $\delta\alpha$. However, a measurement for the duration t_m increases the effective separation by a factor of $\sqrt{\kappa t_m}$, while imperfect quantum efficiency η of the measurement (mainly due to the amplifier noise) increases the Gaussian width by $\eta^{-1/2}$ or, equivalently, decreases the effective separation by $\eta^{-1/2}$. Therefore, we may think about the distinguishability of two Gaussians with width $1/2$ each, separated by

$$\delta\alpha_{eff} = \sqrt{\eta\kappa t_m}\,\delta\alpha, \tag{A37}$$

which gives the error probability due to state separation

$$P_{err}^{sep} = \frac{1 - \mathrm{Erf}(\delta\alpha_{eff}/\sqrt{2})}{2} \approx \frac{\exp[-(\delta\alpha_{eff})^2/2]}{\sqrt{2\pi}\,\delta\alpha_{eff}}. \tag{A38}$$

The other contribution to the measurement error P_{err} for the state $|e\rangle$ comes from the qubit energy relaxation with the rate $\Gamma + T_{1,int}^{-1}$ during the measurement time t_m,

$$P_{err} = P_{err}^{sep} + \tfrac{1}{2}\,t_m\big(\Gamma + T_{1,int}^{-1}\big), \tag{A39}$$

where the factor $1/2$ is because the relaxation moment is distributed practically uniformly within the measurement duration t_m. Since P_{err}^{sep} decreases with time t_m exponentially, the main limitation for P_{err} comes from the second term.

It is easy to find that $P_{err}^{sep} = 10^{-2}$ corresponds to $\delta\alpha_{eff} = 2.3$, $P_{err}^{sep} = 10^{-3}$ corresponds to $\delta\alpha_{eff} = 3.1$, and $P_{err}^{sep} = 10^{-4}$ corresponds to $\delta\alpha_{eff} = 3.7$. For an estimate let us choose $\delta\alpha_{eff} \gtrsim 3$. Then from Eq. (A37) $t_m \gtrsim 9/(\eta\kappa\,\delta\alpha^2)$, and therefore even neglecting intrinsic relaxation $T_{1,int}^{-1}$ in Eq. (A39), we obtain the condition

$$\Gamma \lesssim \tfrac{1}{4}\,P_{err}\eta\kappa(\delta\alpha)^2. \tag{A40}$$

Now using $\Gamma = \kappa g^2/\Delta^2$ and assuming $\kappa \gtrsim 2\,|\chi|$ in Eq. (A36), so that $\delta\alpha \simeq 4\chi\sqrt{\bar n}/\kappa$, we rewrite this condition as

$$\kappa \lesssim 2\sqrt{P_{err}\eta\bar n}\,\frac{|\chi|}{|g|} \simeq 2\sqrt{P_{err}\eta\bar n}\,\frac{|g\delta_q|}{|\Delta|}, \tag{A41}$$

where for the second expression we used $\chi \simeq -g^2\delta_q/\Delta^2$. Since the measurement time t_m should be at least few times longer than κ^{-1}, we obtain

$$t_m > \frac{4}{\kappa} \gtrsim \frac{2}{\sqrt{P_{err}\eta\bar n}}\,\frac{|\Delta|}{|g\delta_q|} = \frac{4/\delta_q}{\sqrt{P_{err}\eta}\sqrt{\bar n/n_{crit}}}. \tag{A42}$$

These estimates show that the Purcell effect requires a sufficiently long measurement time when we desire a small measurement error P_{err}. The limitation is not severe, but it is still inconsistent with a fast accurate measurement needed for quantum error correction. As an example, from Eq. (A42) we see that for $\delta_q/2\pi \simeq 200$ MHz, $P_{err} \simeq 10^{-3}$, $\eta \simeq 0.3$, and $\bar n \simeq n_{crit}/4$ we need $t_m > 400$ ns (this in turn would require a very long $T_{1,int}$). Also, the detuning should be sufficiently

large,

$$|\Delta/g| > \sqrt{\kappa t_m/2P_{err}} > \sqrt{2/P_{err}}, \tag{A43}$$

as directly follows from $\Gamma = \kappa(g/\Delta)^2$ and $\kappa t_m > 4$.

As a more detailed example, let us choose $g/2\pi \simeq 30$ MHz, $\Delta/2\pi \simeq -1.35$ GHz, $\delta_q/2\pi \simeq 200$ MHz, $\kappa^{-1} \simeq 100$ ns, $t_m \simeq 400$ ns, $\eta \simeq 0.3$, and $\bar{n} \simeq n_{crit}/4 \simeq 125$. Then for the excited qubit state the Purcell decay brings the error contribution $t_m\Gamma/2 \simeq 10^{-3}$; the dispersive coupling is $\chi/2\pi \simeq -0.1$ MHz, so $\delta\alpha \simeq 0.25\sqrt{\bar{n}} \simeq 2.8$ and $\delta\alpha_{eff} \simeq 3$, so the separation error is also about 10^{-3} [actually slightly larger since $|\chi|$ decreases with $\bar{n}$ for negative Δ—see Eq. (A30)].

Thus we see that even with the qubit decay due to the Purcell effect, it is possible to measure a qubit with a low measurement error, but this requires a relatively long time and large resonator-qubit detuning. Note that we also had to assume a large number of photons in the resonator, which can lead to detrimental effects (neglected in our analysis) such as dressed dephasing [32,33] and various imperfections related to nonlinear dynamics. Suppression of the Purcell effect (using a Purcell filter or other means) allows us to significantly increase the ratio $|g/\Delta|$, thus increasing the coupling χ and correspondingly decreasing the measurement time for the same measurement error.

[1] M. A. Nielsen and I. L. Chuang, *Quantum Computation and Quantum Information* (Cambridge University Press, Cambridge, 2000).

[2] R. Barends, J. Kelly, A. Megrant, A. Veitia, D. Sank, E. Jeffrey, T. C. White, J. Mutus, A. G. Fowler, B. Campbell, Y. Chen, Z. Chen, B. Chiaro, A. Dunsworth, C. Neill, P. O'Malley, P. Roushan, A. Vainsencher, J. Wenner, A. N. Korotkov, A. N. Cleland, and J. M. Martinis, Nature (London) **508**, 500 (2014).

[3] J. M. Chow, J. M. Gambetta, E. Magesan, D. W. Abraham, A. W. Cross, B. R. Johnson, N. A. Masluk, C. A. Ryan, J. A. Smolin, S. J. Srinivasan, J. Srikanth, and M. Steffen, Nat. Commun. **5**, 4015 (2014).

[4] S. J. Weber, A. Chantasri, J. Dressel, A. N. Jordan, K. W. Murch, and I. Siddiqi, Nature (London) **511**, 570 (2014).

[5] L. Sun, A. Petrenko, Z. Leghtas, B. Vlastakis, G. Kirchmair, K. M. Sliwa, A. Narla, M. Hatridge, S. Shankar, J. Blumoff, L. Frunzio, M. Mirrahimi, M. H. Devoret, and R. J. Schoelkopf, Nature (London) **511**, 444 (2014).

[6] D. Riste, M. Dukalski, C. A. Watson, G. de Lange, M. J. Tiggelman, Y. M. Blanter, K. W. Lehnert, R. N. Schouten, and L. DiCarlo, Nature (London) **502**, 350 (2013).

[7] M. Stern, G. Catelani, Y. Kubo, C. Grezes, A. Bienfait, D. Vion, D. Esteve, and P. Bertet, Phys. Rev. Lett. **113**, 123601 (2014).

[8] J. A. Mlynek, A. A. Abdumalikov, C. Eichler, and A. Wallraff, Nat. Commun. **5**, 5186 (2014).

[9] Z. R. Lin, K. Inomata, K. Koshino, W. D. Oliver, Y. Nakamura, J. S. Tsai, and T. Yamamoto, Nat. Commun. **5**, 4480 (2014).

[10] J. Kelly, R. Barends, A. G. Fowler, A. Megrant, E. Jeffrey, T. C. White, D. Sank, J. Y. Mutus, B. Campbell, Yu Chen, Z. Chen, B. Chiaro, A. Dunsworth, I.-C. Hoi, C. Neill, P. J. J. O'Malley, C. Quintana, P. Roushan, A. Vainsencher, J. Wenner, A. N. Cleland, and J. M. Martinis, Nature (London) **519**, 66 (2015).

[11] A. Blais, R. S. Huang, A. Wallraff, S. M. Girvin, and R. J. Schoelkopf, Phys. Rev. A **69**, 062320 (2004).

[12] A. Wallraff, D. I. Schuster, A. Blais, L. Frunzio, R. S. Huang, J. Majer, S. Kumar, S. M. Girvin, and R. J. Schoelkopf, Nature (London) **431**, 162 (2004).

[13] D. Esteve, M. H. Devoret, and J. M. Martinis, Phys. Rev. B **34**, 158 (1986).

[14] E. M. Purcell, Phys. Rev. **69**, 681 (1946).

[15] H. Haroche and J.-M. Raimond, *Exploring the Quantum: Atoms, Cavities, and Photons* (Oxford University Press, Oxford, 2006).

[16] M. D. Reed, B. R. Johnson, A. A. Houck, L. DiCarlo, J. M. Chow, D. I. Schuster, L. Frunzio, and R. J. Schoelkopf, Appl. Phys. Lett. **96**, 203110 (2010).

[17] E. Jeffrey, D. Sank, J. Y. Mutus, T. C. White, J. Kelly, R. Barends, Y. Chen, Z. Chen, B. Chiaro, A. Dunsworth, A. Megrant, P. J. J. O'Malley, C. Neill, P. Roushan, A. Vainsencher, J. Wenner, A. N. Cleland, and J. M. Martinis, Phys. Rev. Lett. **112**, 190504 (2014).

[18] N. Bronn, A. Corcoles, J. Hertzberg, S. Srinivasan, J. Chow, J. Gambetta, M. Steffen, Y. Liu, and A. Houck, Bull. Am. Phys. Soc. **60**, S39.6 (2015).

[19] N. T. Bronn, E. Magesan, N. A. Masluk, J. M. Chow, J. M. Gambetta, and M. Steffen, arXiv:1504.04353.

[20] J. M. Gambetta, A. A. Houck, and A. Blais, Phys. Rev. Lett. **106**, 030502 (2011).

[21] S. J. Srinivasan, A. J. Hoffman, J. M. Gambetta, and A. A. Houck, Phys. Rev. Lett. **106**, 083601 (2011).

[22] E. A. Sete, A. Galiautdinov, E. Mlinar, J. M. Martinis, and A. N. Korotkov, Phys. Rev. Lett. **110**, 210501 (2013).

[23] E. A. Sete, J. M. Gambetta, and A. N. Korotkov, Phys. Rev. B **89**, 104516 (2014).

[24] J. Koch, T. M. Yu, J. Gambetta, A. A. Houck, D. I. Schuster, J. Majer, A. Blais, M. H. Devoret, S. M. Girvin, and R. J. Schoelkopf, Phys. Rev. A **76**, 042319 (2007).

[25] M. Boissonneault, J. M. Gambetta, and A. Blais, Phys. Rev. Lett. **105**, 100504 (2010).

[26] L. Allen and J. H. Eberly, *Optical Resonance and Two-Level Atoms* (Dover, Mineola, NY, 1997).

[27] The rotating wave approximation neglects the counter-rotating terms. For driven classical oscillators [Eqs. (3) and (4)] it requires that $|\Delta_{rd}|$, $|\Delta_{fd}|$, $|\mathcal{G}|$, and $|\dot{\varepsilon}_r/\varepsilon|$ are small compared to ω_r.

[28] M. O. Scully and M. S. Zubairy, *Quantum Optics* (Cambridge University Press, Cambridge, 1997).

[29] A. N. Korotkov, arXiv:1309.6405, Appendix B.

[30] P. Meystre and M. Surgent III, *Elements of Quantum Optics* (Springer, Berlin, 2007).

[31] H. J. Carmichael, Phys. Rev. Lett. **70**, 2273 (1993).

[32] M. Boissonneault, J. M. Gambetta, and A. Blais, Phys. Rev. A **77**, 060305 (2008).

[33] M. Boissonneault, J. M. Gambetta, and A. Blais, Phys. Rev. A **79**, 013819 (2009).